- Article type: General paper.
- 03/31/2015.
- 7131 words, 2 tables, 12 figures.

Thermal Behavior of Unsaturated Silt at High Suction Magnitudes

Author 1

- Nahed A. Alsherif, Ph.D., Research Associate
- Department of Civil, Environmental, and Architectural Engineering, University of Colorado Boulder, Boulder, CO USA 80309

Author 2

- John S. McCartney, Ph.D., P.E., Associate Professor
- Department of Structural Engineering, University of California San Diego, La Jolla, CA USA 92093-0085

Corresponding author:

John S. McCartney (mccartney@ucsd.edu)

Abstract

A triaxial cell was developed to investigate the shear strength of unsaturated silt under elevated temperatures and high suction magnitudes. The results from a series of drained triaxial compression tests on compacted silt specimens are presented in this paper. After anisotropic compression, some specimens were heated before suction was applied while others were heated after suction application. The shear stress-strain curves of the soils under high suction magnitudes showed a brittle failure mechanism, with a clear increase in peak shear strength with net confining stress. Heating after suction application led to a greater peak shear strength than reference tests at ambient temperature, while heating before suction application led to a lower peak shear strength. Despite the observed path effects, a single peak failure envelope was defined when evaluating the data in terms of effective stress. The suction stress concept was used to define the effective stress, and the values of suction stress were found to be linked with a nonisothermal definition of the soil-water retention curve.

Keywords

Unsaturated soil; shear strength; temperature; high suction

List of notation

c	is the apparent cohesion
e_o	is the initial void ratio
M_W	is the molecular mass of water vapour
M_{CSL}	is the slope of the critical state line
M_{peak}	is the slope of the peak failure envelope
N	is a reference specific volume point on the virgin compression line
N_{vG}	is an empirical parameter of the van Genuchten (1980) soil-water retention curve
p	is the mean total stress
p'	is the mean effective stress
R_h	is the relative humidity of the pore air in decimal form
R	is the universal (molar) gas constant
T	is the temperature
T_f	is a final observed temperature
T_r	is a reference temperature
u_w	is the pore water pressure
u_a	is the pore air pressure
v_κ	is a reference specific volume point on the recompression line
α_{GS}	is an empirical parameter of the Grant and Salehzadeh (1996) soil-water retention curve
α_{vG}	is an empirical parameter of the van Genuchten (1980) soil-water retention curve
β_0	is an empirical parameter of the Grant and Salehzadeh (1996) soil-water retention curve
ΔT	is the change in temperature
ε_v^p	is the plastic volumetric strain
ϕ'	is the effective friction angle
λ	is the slope of the virgin compression line
λ_{GS}	is an empirical parameter of the Grant and Salehzadeh (1996) soil-water retention curve
κ	is the slope of the recompression line

ρ_w is the density of water

σ_s is the suction stress

σ' is the effective stress

σ is the total stress

σ_n is the net stress

ψ is the suction

ψ_{aev} is the air entry suction

Ω is an effective stress scaling parameter in the model of Khalili and Khabbaz (1998)

1. Introduction

An improved understanding of the thermo-hydro-mechanical behaviour of unsaturated soils during application of elevated temperatures and high suction magnitudes is needed to interpret the behaviour of thermally-active geotechnical systems located above the water table. Examples of these systems include ground-source heat exchangers (Preene and Powrie 2009), energy foundation systems (Brandl 2006; Laloui et al. 2006; Adam and Markiewicz 2009; Bourne-Webb et al. 2009; Murphy et al. 2015), heat dissipation embankments (McCartney 2012; Coccia and McCartney 2013; Stewart et al. 2014), containment systems for nuclear waste (Gens et al. 1998; Kanno et al. 1999), and backfills for buried electrical cables (Abdel-Hadi and Mitchell 1981; Brandon et al. 1989). When these thermally-active geothermal systems are operated in heating mode, thermally-induced water flow may cause the unsaturated soil surrounding the heat exchangers to dry to the point that very high suction magnitudes may be encountered.

The shear strength and volume change behaviour of unsaturated soils under high suction magnitudes due to changes in temperature remain largely uncertain due to the lack of supporting experimental data in the literature. Although data is available on the thermo-hydro-mechanical response of compacted silt under low suction magnitudes (Uchaipichat and Khalili 2009), the behaviour of compacted silt under high suctions may differ. Specifically, the pore water under very low degrees of saturation (less than 5%) may have different effects on the effective stress state and the thermal volume change response than under higher degrees of saturation. Small changes in volume of the pore water during temperature changes may lead to large changes in suction at the tail-end of the soil-water retention curve (SWRC), and the soil may retain less water under high temperatures (Grant and Salehzadeh 1996; Romero et al. 2003). Further, the role of suction and degree of saturation in the definition of effective stress at high suction magnitudes and nonisothermal conditions is uncertain, as most studies linking these variables involved verification using results from tests involving suction magnitudes less than 500 kPa (Khalili and Khabbaz 1998; Lu et al. 2010). Due to the lack of experimental data on shear strength and volume change under high suctions and nonisothermal conditions, the suitability of extending effective stress-based thermo-elasto-plastic constitutive relationships developed for saturated soils to unsaturated conditions has not been assessed.

The primary objective of this study is to understand the impact of temperature on the shear strength and deformation behaviour of compacted, unsaturated silt specimens under high suction magnitudes. Specifically, this study involves an investigation into the effects of change in temperature on the SWRC, volume change response, shear-stress strain curves, and failure envelopes of unsaturated soils under high suction magnitudes. To accomplish the objective of this study, a new triaxial cell was developed to measure the shear strength of unsaturated soils under elevated temperatures and high suction magnitudes. Specifically, the vapour flow technique developed by Likos and Lu (2003) was employed in the triaxial cell to control the total

suction in the specimen, along with a temperature control system to apply elevated temperatures. The details of the triaxial cell were defined based on the experience of Uchaipichat et al. (2011), including the use of a set of resistance heaters within the triaxial cell, a glass pressure cell, cell fluid circulation, and redundant approaches to measure specimen volume change.

2. Background

2.1 Influence of Temperature on SWRC

The effect of temperature on the SWRC of compacted soils under high suction magnitudes has been investigated in several studies. This is important to consider as changes in the SWRC may affect the mechanical behaviour of unsaturated soils (Romero et al. 2001; Uchaipichat and Khalili 2009). Studies in the area of soil physics by Grant and Salehzadeh (1996) and She and Sleep (1998) observed that an increase in temperature leads to a decrease in degree of saturation for a given suction. They attributed this shift to changes in the soil-water contact angle, a reduction in the interfacial tension between air and water, and thermal expansion of air entrapped within the soil pores. They observed that the change in contact angle primarily led to a reduction in the air entry suction. A shift in the SWRC to lower degrees of saturation for elevated temperatures was also reported in studies by geotechnical engineers that involved control of the stress state and measurement of volume change, including Romero et al. (2001), Salager et al. (2007), and Uchaipichat and Khalili (2009) for low suction values and Olchitzky (2002), Romero et al. (2003), Imbert et al. (2005), Tang and Cui (2005), and Villar and Gomez (2007) for high suction values. Romero et al. (2003) found that the density of the soil does not affect the SWRC at low degrees of saturation. Olchitzky (2002) compared his results with a prediction based on a reduced interfacial tension, and found that this reduction was not sufficient to explain the change in water retention with temperature. Uchaipichat and Khalili (2009) observed that the SWRC under different temperatures is independent of stress state for low suction magnitudes.

2.2 Thermal Volume Change Behaviour of Unsaturated Soils

The volume change behaviour of unsaturated soils during heating has been investigated in several studies (Romero et al. 2003; Francois et al. 2005; Salager et al. 2008; Tang et al. 2008; Uchaipichat and Khalili 2009). Tang et al. (2008) performed thermo-mechanical tests on unsaturated, heavily-compacted MX80 bentonite following a wetting path from an initial suction of 110 MPa to a target suction of 9 MPa. The results from tests at constant confining stress showed that heating led to expansion under low values of confining stress and high suction, and led to contraction at high values of confining stress and low suction. This indicates that stress history plays an important role in the thermal response of unsaturated soils in a similar manner to that observed for saturated soils (Baldi et al. 1988). Uchaipichat and Khalili (2009) performed drained heating tests on silt specimens at matric suctions up to 300 kPa and net confining stresses up to 200 kPa, and found that heavily overconsolidated specimens experienced

reversible thermal expansion with introducing larger irreversible thermal contraction at lower overconsolidation ratio. Further, for a given net mean stress, the amount of thermal contraction increased with increasing suction.

2.3 Effect of Temperature on the Shear Strength of Soils

The influence of temperature change on the shear strength and stress-strain characteristics of saturated soils have been studied by several investigators. Houston et al. (1985) performed consolidated undrained tests on saturated, normally consolidated specimens of Illite clay at different temperatures, and observed that the pore water pressure increased and effective stress decreased during heating. However, after drainage of these thermally-induced excess pore water pressures, the peak shear strength of the soil was greater than at low temperatures. Hueckel and Baldi (1990) performed drained triaxial compression tests on overconsolidated specimens of Pontida silty clay, and observed a decrease in peak shear strength with temperature. This was attributed to a reduction in the size of the yield locus (and consequently a reduction in the overconsolidation ratio), but it may also be related to the increase in void ratio during heating of the overconsolidated soil. The uniqueness of the critical state line (CSL) was also investigated and confirmed by Hueckel and Baldi (1990) and Graham et al. (1995). These studies also observed that temperature has a negligible effect on the critical state line.

Uchaipichat and Khalili (2009) evaluated the shear strength and volume change of unsaturated compacted silt under non-isothermal conditions for suction magnitudes less than 300 kPa. For a given suction magnitude, they observed a decrease in peak shear strength with increasing temperature. However, the shear strength at critical state conditions was unaffected by temperature, similar to the conclusions drawn for saturated clays. They observed that changes in matric suction led to greater changes in the peak and critical state strength values than changes in temperature. Similar reductions in peak shear strength and increases in shear strength with suction were observed by Wiebe et al. (1998) and Ghembaza et al. (2007b). Wiebe et al. (1998) prepared specimens of sand-bentonite at different degrees of saturation using compaction at different water content, which could have led to different soil structures, but Ghembaza et al. (2007b) incorporated the vapour equilibrium technique into a triaxial cell to perform triaxial compression tests on normally consolidated, unsaturated sandy clay under a temperature of 80°C and a suction value of 8.5 MPa.

3. Experimental Technique

3.1 Testing Apparatus

The new triaxial testing setup consists of three main components: a suction control system, a temperature control system, and a mechanical loading system. A schematic of the triaxial testing setup is shown in Figure 1. The suction control system consists of a gas flow control system with relative humidity feedback, which was designed to permit automated control of the relative humidity of the pore air being supplied to the base of the soil specimen, and

consequently control of the total suction applied to the soil specimen. The total suction in the specimen can be calculated using Kelvin's law, as follows:

$$\psi = \frac{\rho_w RT}{M_w} \ln\left(R_h\right)$$

1.

The molecular mass of water vapour, M_w, is assumed equal to 18.016 g/mol, and the universal (molar) gas constant, R, is equal to 8.31432 J/molK, ρ_w is the density of water, T is the temperature in kelvin, R_h is the relative humidity in percent. The temperature control system consists of three heating elements impeded inside the triaxial cell, a temperature control unit, a thermocouple installed through the top of the cell, and a pump to circulate the pressurized water inside the cell. The temperature control system were used to control the target elevated temperature applied to the cell water and soil specimen, and to ensure uniform temperature distributions. The mechanical loading system was adapted to operate in load-control conditions during suction application or temperature changes or in displacement-control conditions during shearing of the soil specimen. In either configuration, a load cell is used to record axial loads, and a linearly variable differential transformer (LVDT) is used to track axial displacements. The volume change of the soil specimen during changes in suction, temperature, or shearing is also monitored by recording the water level in a graduated burette connected to the water supply line of the cell pressure using a differential pressure transducer. A detailed description of the testing apparatus can be found in Alsherif and McCartney (2014a; 2014b).

3.2 Materials and Specimen Preparation

Silt obtained from the Bonny dam on the Colorado-Kansas border (Bonny silt) was used in this experimental study. As the behaviour of the silt under compacted conditions was evaluated in this study, modified and standard Proctor compaction tests were performed on Bonny silt at a room temperature of 23 °C. The compaction curves along with the zero air voids (ZAV) line are shown in Figure 2(a). Bonny silt has a specific gravity of 2.65. The drying-path soil water retention curve (SWRC) at a temperature of 23 °C for Bonny silt compacted to a void ratio of 0.68 is shown in Figure 2(b). Data points from saturated conditions until the point at which the water phase became discontinuous (i.e., where water could no longer be extracted from the specimen) were obtained using the flexible-wall permeameter setup developed by McCartney and Znidarčić (2010), which occurred at a degree of saturation of about 0.65. In addition to the low suction data, two data points from high suction magnitudes obtained using the vapour flow technique and corresponding to the conditions investigated in this study are shown in Figure 2(b). The van Genuchten (1980) SWRC model was fitted to the data using the approach of Alsherif and McCartney (2014a), which involved a minor adjustment of the N_{vG} parameter to match the SWRC data while still providing a good prediction of the suction stress characteristic curve (SSCC) at ambient temperature using the model of Lu et al. (2010). The shape of the

WRC can be extrapolated by fitting the model to the data at low and high suction values. The compression response of an unsaturated Bonny silt specimen under as-compacted conditions was assessed using a constant water content oedometer test, with loading increments applied until settlement was negligible. The compression curve is shown in Figure 2(c), along with an estimate of the preconsolidation stress. The final water content of the soil specimen indicated negligible evaporation.

To prepare a specimen for testing in the triaxial cell, moisture-conditioned Bonny silt was statically compacted using a press in three lifts having thicknesses of 24 mm in a 35 mm-diameter mould. The interfaces between lifts were scarified. The specimens had a dry unit weight of 15.7 kN/m^3 and initial degree of saturation of 0.41, which corresponds to an initial void ratio of approximately 0.68 and a compaction water content of 10.5% (8% dry of optimum). The low compaction water content was selected so that the initial degree of saturation was low enough to have continuous air voids through the specimen (approximately 40%). In this case, the air permeability is expected to be high enough to permit rapid suction equilibration using the vapour flow technique.

3.3 Testing Procedures

After assembly of the triaxial cell, all of the tests performed in this study start with application of a confining stress (100, 200 or 300 kPa) and K_0 consolidation under as-compacted conditions, using a value of K_0 of 0.5 that corresponds approximately with the value calculated from Jaky's equation and the friction angle of the compacted silt. The average air pressure in the specimens is approximately 20 kPa, so the net confining stress values were 20 kPa smaller than the cell pressure. Next, tests following four different paths were performed to understand the effects of suction and temperature on the volume change and shear strength behaviour of compacted Bonny silt. The different testing paths are illustrated in Figure 3. The first set of tests was performed by applying a high suction magnitude to soil specimens under ambient laboratory temperature (approximately 23 °C), as shown in Figure 3(a). This set of tests provides a baseline case for the behaviour of Bonny silt under high suction values. The second set of tests were performed by heating soil specimens to a target cell fluid temperature of 65 °C in a single stage under as-compacted conditions, then applying a high suction magnitude as shown in Figure 3(b). Tests following this procedure are referred to as T-S (temperature-suction) path tests. The third set of tests were performed by applying a suction magnitude to the soil specimens under ambient temperature, then heating them in three stages to target cell fluid temperatures of 35, 50, and 65 °C, as shown in Figure 3(c). Tests following this procedure are referred to as S-T (suction-temperature) path tests. Finally, a fourth type of test was performed following the S-T path but was cooled back to ambient temperature after heating, as shown in Figure 3(d). The initial conditions for the specimens evaluated in the triaxial compression testing program are presented in Table 1.

After following any of the testing paths, the soil specimens were sheared at a constant displacement rate of 1.27×10^{-4} m/min. Although this rate is relatively fast for a drained test, as no change in relative humidity at the boundaries was noted during shear it was assumed to correspond to drained conditions. The unsaturated specimens evaluated in this study have degrees of saturation of around 0.06, which is very close to the residual degree of saturation. Accordingly, it is not expected that there is sufficient water in the pores to become pressurized during the shearing process and affects the effective stress state. Further, the relative humidity control system was operated during shearing (i.e., free drainage of air), which ensures that the suction remained constant during shearing. More details on specimen setup and test procedures can be found in Alsherif and McCartney (2014b).

4. Results

4.1 Results of Suction Equilibration

Examples of the relative humidity and temperature at the bottom and top of two specimens during suction equilibrium for tests following the T-S and S-T paths are shown in Figures 4(a) and 4(b), respectively. The temperature at the bottom of the specimen (T_{bottom}) was very stable during suction application, and was 64 °C for the test following the T-S path and 23 °C for the test following the S-T path. Although the temperature at the top of the specimen was not measured, the temperature of the gas flowing out of the top of the specimen ($T_{outflow}$) was measured within the insulated flask. Despite the insulation of the flask, the outflow temperature was sensitive to the room temperature due to the presence of the vent. For the example test shown in Figure 4(a), the outflow temperature stabilized at 61 °C after the relative humidity of the outflow gas stabilized. At this point the outflow rate is also stable. In both tests, approximately two hours were needed for the relative humidity at the bottom ($R_{h\ bottom}$) to reach the target value ($R_{h\ target}$), while an average of one to two weeks was needed for the relative humidity at the top ($R_{h\ top}$) to reach the same target value. Specifically, 90% of the completely dry Nitrogen gas ($N_{2\ dry}$) was mixed with 10% of the water vapour-saturated Nitrogen gas ($N_{2\ wet}$) to reach the target relative humidity of 15% at equilibrium conditions in Figure 4(a), while 88% of $N_{2\ dry}$ was mixed with 12% of $N_{2\ wet}$ to reach the target relative humidity of 12% in Figure 4(b). The target relative humidity for the tests following the T-S path was slightly different than the tests following the S-T path because the total suction calculated using Kelvin's law is sensitive to temperature. Although the target suction was 291 MPa for all of the nonisothermal tests, the suction in the tests following the T-S path was 317 MPa due to difficulty in reaching the exact target relative humidity that corresponds the target suction. Nonetheless, both suction values are within residual saturation conditions for Bonny silt, so it is assumed that they are close enough for comparison. After the target relative humidity at the top of the soil specimen was attained and the differential pressure across the soil specimen was constant, the suction was maintained for at least six additional hours to ensure uniformity of total suction throughout the specimen.

4.2 Results of Thermal Volume Change

The volumetric strains as a function of the change in cell fluid temperature for different testing paths and confining stresses are presented in Figure 5. When following the T-S path, the soil specimens were heated in a single stage at a constant heating rate of 10.5 to 11.5 °C/hour. The thermal axial strains for the unsaturated silt specimens following this path shown in Figure 5(a) indicate that the specimens initially expanded during heating before contracting at higher temperatures. Greater contraction with increasing confining stress was observed at the highest temperature evaluated. Uniform contraction was observed in the thermal volumetric strains for these specimens in Figure 5(b). The soil specimens in the tests following the T-S path were heated under as-compacted conditions (initial S_r of 0.41) before application of suction. In this case, heating likely causes generation of excess pore water pressure, which drained and resulted in permanent contraction. The slight axial expansion of the specimens tested under lower confining stresses may have occurred due either transient drainage effects that did not have time to fully dissipate, or heating of the lightly overconsolidated specimens above the contraction threshold temperature observed by Hueckel and Baldi (1990). The difference in the trends in thermal axial and volumetric strains with the change in temperature may also have occurred due to the effects of the anisotropic stress state as observed by Coccia and McCartney (2012). Specifically, the trend in the thermal axial strains is similar to that expected for lightly overconsolidated soils while the trend in the thermal volumetric strain is similar to that expected for normally consolidated soils.

The thermal axial strains following the S-T path shown in Figure 5(c) differ from those following the T-S path, and show expansion during staged heating similar to heavily overconsolidated soils heated below the contraction threshold temperature (Hueckel and Baldi 1990; Delage et al. 2000, 2004; Cekeravac and Laloui 2004). Similar trends in volumetric expansion are also observed for these specimens, as shown in Figure 5(d). After application of high suction magnitudes, these specimens have a degree of saturation of approximately 0.06 prior to heating, so it is unlikely that there is significant generation of excess pore water pressures. Application of high suction magnitudes likely results in an increase in mean effective stress, as well as an increase in mean preconsolidation stress. If the increase in preconsolidation stress is greater than the effective stress, this would lead to an increase in the OCR causing the silt to behave like a heavily overconsolidated soil. Further, application of high suction values lead to a reduction in volume (which will be discussed later). Despite the relatively low water content of the soils following the S-T path, the results in Figures 5(c) and 5(d) indicate that stress history still plays an important role in the thermal volume change of unsaturated soils under high suction magnitudes.

4.3 Results of Triaxial Compression Testing

The stress-strain curves for the soil specimens that had reached thermal equilibrium following different testing paths are shown in Figure 6. The shear stress-strain curves for the specimens

tested at different temperatures and suctions following different paths, for cell pressures of 100, 200, and 300 kPa are shown in Figures 6(a), 6(b), and 6(c), respectively. A brittle failure mode was observed in the stress-strain curves for all specimens under high suction magnitudes regardless of the temperature. A sharp drop in the applied shear stress was noticed after reaching the peak shear strength. A clear failure plane was observed as well, and the specimen broke into two pieces. This failure mode differed significantly from the relatively ductile failure mode observed in tests on saturated conditions tested in isotropic consolidated-undrained triaxial compression tests reported by Alsherif and McCartney (2014a). Because of the brittle failure mode, it was not possible to shear the specimens tested under high suction magnitudes to critical state conditions. The results in Figure 6 indicate that the peak shear strength of the specimens tested following the T-S path was consistently smaller than those tested under ambient temperature conditions, while the peak shear strength of the specimens tested following the S-T path was greater. A summary of the results from the triaxial compression tests on unsaturated specimens at different high suction magnitudes, temperatures, and testing paths are presented in Table 2. The temperatures measured using the relative humidity probe below the specimen were slightly lower than the target cell fluid temperature, which was 65 °C.

The volumetric strains during shearing of the unsaturated specimens at various confining stresses following the T-S path and the S-T path are shown in Figures 7(a) and 7(b), respectively. The black points correspond to the points of peak shear strength. The results indicate that specimens tested following the T-S and S-T paths dilate during shear. Although an unclear trend with confining pressure was observed for the specimens tested following the T-S path, the specimens sheared following the S-T path tests experienced a similar amount of dilation for all three normal stresses.

A summary of the void ratios at different stages of tests performed at ambient temperature is shown in Figure 8(a). The void ratio is observed to decrease during application of confining stresses, as well as during application of a suction of 291 MPa. A small amount of dilation is observed after shearing. A summary of the void ratios at different stages of the tests following the T-S path is shown in Figure 8(b). In these tests, a similar reduction in void ratio is observed during application of the confining stress. A slight reduction in void ratio during heating corresponding to the thermal volumetric contraction of less than 1% shown in Figure 5(a) is then observed. The specimens contracted further during application of a suction of 291 MPa, and dilated slightly during shearing. The summary of the void ratio values at different stages of the tests following the S-T path at different confining stresses is shown in Figure 8(c). The results in this figure clearly indicate that the void ratio was sensitive to the confining stress and applied suction, similar to the results in Figure 8(a). However, heating of the specimen after it was in equilibrium at a suction of 291 MPa led to expansion of the soil specimens, which was followed by further expansion due to dilation during shearing. A comparison of the void ratio values prior to shearing in Figures 8(a), 8(b) and 8(c) indicates lower void ratios for the tests following the

S-T path than those for the tests at ambient temperature and those following the T-S path. This may partially explain the greater peak shear strength values observed for the tests following the S-T path. The void ratio of the specimen which experienced a heating and cooling cycle after reaching suction equilibration is shown in Figure 8(c). Although there is a slight variability compared to the other test performed at a confining stress of 300 kPa, the void ratio at stage four for this test reflects a net contraction the specimen after cooling back to ambient temperature.

The impact of temperature on the void ratio at failure as a function of the peak principal stress difference for different testing paths is shown in Figure 9. Overall, the data points follow a similar trend, which confirms that the peak shear strength is sensitive to the density of the soil at failure. However, it should be noted that the void ratio at failure for the saturated specimens at ambient temperature were at critical state conditions, while the void ratio at peak failure conditions for the unsaturated specimens at high suction magnitudes were not at critical state conditions due to the brittle failure mode.

5. Analysis and Discussion

5.1 Effective Stress Evaluation of the Peak Shear Strength of Specimens at High Suction and High Temperature

The drained failure envelopes for the specimens tested at ambient temperature and those tested following the T-S and S-T paths are shown in Figure 10(a). The peak shear strength increases linearly with net confining stress, and the total friction angle appears to not be affected by temperature or suction. However, the apparent cohesion in this total stress plot was affected by changes in both temperature and suction. Despite having a slightly greater suction magnitude, the specimens following the T-S path consistently have a lower peak shear strength than the specimens tested at ambient temperature and a suction of 291 MPa. This may imply that the softening effect due to heating at a relatively high degree of saturation observed by Uchaipichat and Khalili (2009) was greater than the hardening effect associated with suction application. This behaviour is consistent with the observations of Hueckel and Baldi (1990) for the effects of temperature on the peak shear strength of saturated, heavily-overconsolidated clay. In contrast, the specimens tested following the S-T path consistently have a greater peak shear strength than the specimens tested at ambient temperature, which was not expected. Although the results in Figure 8 indicate that there is some variability in the void ratio at the end of suction application for the ambient temperature tests and those following the S-T path, the specimens tested following the S-T path have a slightly greater void ratio than the specimens tested at ambient temperature due to the thermal expansion. A greater void ratio should have led to a lower shear strength, but this was not the case. Another difference between these two sets of tests was the lower degree of saturation for the tests following the S-T path due to drying during heating.

The greater shear strength values of the specimens tested following the S-T path indicate that the degree of saturation may have the opposite effect on the stress state at high suction magnitudes and high temperatures than that expected at low suction magnitudes. At low suctions, a decrease in the degree of saturation implies that there is less water available to hold the particles together by capillarity. Heating of a soil under relatively dry conditions (high suctions) may cause the water in adsorbed films to expand and collect around the particle contacts leading to greater particle interaction. For the test performed following the S-T path with a heating-cooling cycle, the peak shear strength was found to be slightly higher than that from the test performed at the same confining stress and suction that had not experienced heating. This gain in peak shear strength can be attributed to the slightly greater decrease in void ratio during suction application, as well as the slight permanent contraction upon cooling.

Regardless of the testing path, the compacted silt specimens under high suction magnitudes still show a frictional response in which the peak shear strength increases with the confining pressure. Because of this frictional response, the principle of effective stress may still be valid for these soils despite the high suction magnitude and brittle failure mechanism. The effective stress was defined in this study using the suction stress characteristic curve (SSCC) proposed by Lu and Likos (2006), which is a functional relationship between suction stress and suction for a given soil under a certain stress state. The suction stress σ_s is assumed to represent the net effect of the different inter-particle stresses in unsaturated soils. Assuming that the friction angle is constant, the suction stress can be back-calculated from a linear failure envelope by assuming that it is equal to the apparent tensile strength (Lu and Likos 2006), as follows:

$$\sigma_s = \frac{c}{\tan(\varphi')} \quad (2)$$

where *c* is the apparent cohesion, ϕ' is the effective friction angle. The mean effective stress can be calculated from the suction stress as follows:

$$p' = \left(p - u_a\right) + \sigma_s \quad (3)$$

where p is the mean total stress, u_a is the pore air pressure. This approach is similar to that of Bishop (1959), where σ_s is the product of the suction ψ and an effective stress parameter χ that describes the impact of suction on the effective stress during changes in degree of saturation. The conceptual advantage of using the SSCC approach is that it shows that the suction stress is a functional relationship governing the mechanical response of unsaturated soils in a similar manner to which the SWRC governs the hydraulic response of unsaturated soils. Lu and Likos

(2006) validated the SSCC concept by re-examining shear strength data of unsaturated soils (up to a suction of 1500 kPa) from the literature in terms of Equation (3), and found that the failure envelopes for unsaturated specimens converge with that for saturated specimens.

The drained failure envelopes for the unsaturated specimens shown in Figure 10(a) were used to back-calculate four different values of suction stress σ_s using Equation (2) for each of the different testing paths evaluated. The different suction stress values, summarised in Table 2, indicate that the SSCC depends on temperature similar to the SWRC, but also on the testing path. Despite the high suction magnitudes considered in this study, the magnitudes of experimental suction stress listed in Table 2 are on the same order of magnitude as the mean net stress at the beginning of shearing, which explains why the soil exhibits the frictional response observed in Figure 10(a). In other words, the high suction magnitude still has an impact on the effective stress, but it is diminished by the small amount of water in the soil.

The peak shear strength values plotted as a function of the mean effective stress calculated using the experimentally-derived suction stress values are shown in Figure 10(b). Regardless of the temperature and testing path, the peak shear strength values define a single peak failure envelope having a slope of M = 2.1. Shear strength values from isotropic consolidated undrained tests on saturated specimens (zero suction tests) reported by Alsherif and McCartney (2014b) are also shown in this figure, along with the critical state line (CSL) fitted to these data points. The CSL was extrapolated to higher mean effective stresses for comparison purposes. It is clear that the peak failure envelope is steeper than the CSL, confirming that the brittle failure mechanism prevented the unsaturated specimens from reaching critical state. Nonetheless, the fact that the peak shear strength values for specimens with elevated temperatures and high suction magnitudes converge on a single failure envelope in mean effective stress space supports the validity of the effective stress principle for these relatively extreme conditions. The behaviour of the specimens at high suctions is consistent with that of heavily overconsolidated soils, which reach a peak shear strength value when the effective stress path intersects the steady-state boundary surface.

To better interpret the impact of testing path on the behaviour of unsaturated specimens tested following the T-S and S-T paths, the secant moduli at an axial strain of 0.5% (which are assumed to represent elastic conditions) were calculated from the shear stress-strain curves in Figure 6. The change in secant moduli for the specimens sheared under elevated temperature with respect to the moduli for the specimens tested at a similar net confining stress and ambient temperature is shown in Figure 11. In general, specimens that were heated after application of high suction (S-T path) experienced an increase in secant modulus, while those that were heated under as-compacted conditions followed by application of high suction do not experience a significant change in secant modulus except at low net confining stresses. This increase in secant modulus may be attributed to the further removal of pore water during

heating in the tests following the S-T path, which had a degree of saturation that was 3% lower than the other tests. This explanation indicates that a reduction in the degree of saturation when heating soils near residual saturation induces hardening and an increase in stiffness.

5.2 Constitutive Modelling of Temperature Effects on the SWRC and SSCC

As the suction stress concept was found to be useful in interpreting the shear strength of the specimens tested under different temperatures and following different paths, linkages between the SWRC and SSCC for high suctions and temperatures were explored. The SSCC can be defined using many different approaches, including the product of the degree of saturation and suction (Bishop 1959), the product of effective saturation and suction (Lu et al. 2010), and empirical relationships involving characteristic points on the SWRC like the air entry suction (Khalili and Khabbaz 1998). Lu et al. (2010) found that defining the SSCC as the product of the effective saturation and suction can represent the behaviour of both sand and clay, and the use of the effective saturation permits many SWRC models to be directly integrated into the SSCC. Accordingly, the first linkage between the SSCC and the SWRC was performed using the nonisothermal SWRC model of Grant and Salehzadeh (1996), which is given as follows:

$$S_e = \frac{S_r - S_{r,res}}{1 - S_{r,res}} = \left\{ \frac{1}{\left[\alpha_{GS} \psi_{(T=T_r)} \left(\frac{\beta_0 + T_r}{\beta_0 + T_f} \right) \right]^{\lambda_{GS}} + 1} \right\}^{\frac{(\lambda_{GS}-1)}{\lambda_{GS}}}$$

4.

The values of T_r and T_f in this equation are the reference and final temperatures before and after heating, respectively and should be defined in Kelvin. A value of the empirical parameter β_0 of -400 K was used in this analysis as Grant and Salehzadeh (1996) and She and Sleep (2008) observed that this was a reasonable value for silts during drainage. The results of this model for an initial temperature of T_r = 296 K and final temperatures of T_f = 296 K (ambient temperature tests) and 337 K (elevated temperature tests) are shown in Figure 12(a). The Grant and Salehzadeh (1996) model corresponds well with the SWRC points at ambient temperature from Figure 2. For elevated temperatures, the Grant and Salehzadeh (1996) model predicts a decrease in the air entry suction, and an overall downward shift in the SWRC in the direction of lower degrees of saturation. One issue with the model is that it cannot capture the decrease in residual water content with temperature that is observed in the data. The SSCC defined from the Grant and Salehzadeh (1996) SWRC is given as follows:

$$\sigma_s = (u_a - u_w) S_e = (u_a - u_w) \left\{ \frac{1}{\left[\alpha_{GS} \psi_{(T=T_r)} \left(\frac{\beta_0 + T_r}{\beta_0 + T_f} \right) \right]^{\lambda_{GS}} + 1} \right\}^{\frac{(\lambda_{GS}-1)}{\lambda_{GS}}}$$

5.

The SSCCs predicted using the parameters of the Grant and Salehzadeh (1996) SWRC model reported in Figure 12(a) are presented in Figure 12(b). The experimental suction stress points from Table 2 are also shown in this figure for comparison. The SSCC predicted from the Grant and Salehzadeh (1996) model correspond well with the points from the ambient temperature tests and the T-S path tests. The lower values of degree of saturation predicted using the Grant and Salehzadeh (1996) model at elevated temperatures lead to a decrease in suction stress, albeit by a greater amount than that observed in the experiments. Alternatively, the SSCC can also be characterized using the suction stress defined using the model of Khalili and Khabbaz (1998), given as follows:

$$\sigma_s = \psi \left\{ \frac{\psi}{\psi_{aev}} \right\}^{-\Omega}$$

6.

where ψ is the suction, ψ_{aev} is the air entry suction, and Ω is an effective stress scaling parameter. Khalili and Khabbaz (1998) found that a value of Ω = -0.55 fits well for most experimental data. The SSCCs predicted with Equation 6 using the air entry suction values from the Grant and Salehzadeh (1996) SWRC curves shown in Figure 12(a) are also shown in Figure 12(b). This model has a slightly different trend in suction stress with increasing suction, and generally provides a better fit to the ambient temperature and T-S path data. A comparison between the experimental suction stress values with those predicted using Equation 6 with the air entry suction values from Figure 12(a) is shown in Figure 12(c).

Although Equation 6 provides a good match for the specimens tested at ambient temperature and following the T-S path, it is clear that it underestimates the suction stress for the specimens tested following the S-T path. A possible explanation is that the specimens tested following the S-T path may have experienced a reduction in the pore size distribution during the volumetric contraction associated with application of high suction magnitudes, leading to an increase in the air entry suction (Ng and Pang 2000). Further changes may have occurred due to drying during heating, leading to a greater air entry suction than at ambient temperature. A greater value of air entry suction of 1.17 kPa was found to provide a good fit to the experimental suction stress

value for the S-T path tests using Equation 6. This data point is also plotted in Figure 12(c). More research is required to fully understand the effects that the nonisothermal S-T testing path may have on the shape of the SWRC, and in how transitions in the shape of the SWRC relate to changes in effective stress.

6. Conclusion

Drained triaxial compression tests were performed on specimens of compacted silt using a new triaxial cell following different testing paths to investigate the influence of temperature on the shear strength and volume change behaviour of unsaturated, compacted silt. The specific conclusions regarding the behaviour of compacted silt under high temperatures and suctions that can be drawn from this study are as follows:

- The thermal volume change was found to depend on the initial overconsolidation ratio of the unsaturated silt specimens prior to heating. Unsaturated silt specimens heated prior to suction implementation (T-S path) had an initially low overconsolidation ratio and experienced thermal contraction during heating. Unsaturated silt specimens heated after reaching suction equilibrium (S-T path) had a high overconsolidation ratio prior to heating, and experienced thermal expansion during heating.
- The shear stress-strain curves for all of the specimens tested at high suction magnitudes show a brittle failure mechanism that differed significantly from the shear stress-strains of the same soil sheared under saturated conditions. Because of this brittle failure mechanism, the unsaturated soil specimens could not be sheared until reaching critical state conditions.
- If a suction value was imposed after heating, the shear strength was observed to decrease by 10% during a change in temperature of approximately 41 °C. If a suction value was imposed before heating, the shear strength was observed to increase by 20% during the same change in temperature.
- Silt specimens heated under as-compacted conditions before application of a high suction value experienced thermal softening that led to lower peak shear strength values than those measured in tests on specimens at high suction magnitudes performed under ambient temperature. This behavior was consistent with that expected in the literature for overconsolidated soils.
- Greater peak shear strength values and greater secant moduli values were observed for specimens that were heated under high suction magnitudes than those observed for tests on soils at high suction magnitudes under room temperature conditions. This unexpected behaviour was attributed to the lower degree of saturation of the specimens tested following the S-T path, and it is hypothesized that the degree of saturation has a different effect on the stress state at high suction magnitudes near residual saturation conditions than for nearly-saturated soils.
- The suction stress components of the effective stress were interpreted from the peak failure envelopes in mean net stress space, which permitted definition of a single peak failure

envelope in effective stress space that represented the shear strength behaviour of the compacted silt at different temperatures, suctions, and following different testing paths. The slope of this peak failure envelope was greater than the slope of the critical state line defined from tests on saturated specimens.

- The data obtained from tests on specimens at high suction magnitudes indicated a shift in the SWRC to a lower degree of saturation with elevated temperatures. The nonisothermal SWRC model of Grant and Salehzadeh (1996) also indicated a shift in the SWRC to a lower degree of saturation, although not at high suction magnitudes. A reduction in the air entry suction with temperature was observed, which has an important effect on the effective stress.
- Different approaches were used to predict the change in suction stress with temperature. The approach of Khalili and Khabbaz (1998) that uses the air entry suction as a key parameter to define the suction stress was observed to provide a good fit to the suction stress for the specimens sheared at ambient temperature and following the T-S path. The approach using the product of the suction and effective saturation to define the suction stress also provided a good fit. Neither approach was suitable to predict the increase in suction stress for specimens following the S-T path. However, a possible explanation is that suction application at ambient temperature followed by further drying during heating may have led to a change in the pore size distribution that caused an increase in the air entry suction compared to the ambient temperature tests.

Acknowledgements

This material is based upon work supported by the National Science Foundation (NSF) under Grant CMMI 1054190. Any opinions, findings, and conclusions or recommendations expressed in this material are those of the authors and do not necessarily reflect the views of NSF. The first author would also like to acknowledge funding from the Libyan government.

References

Abdel-Hadi ON and Mitchell JK (1981) Coupled heat and hater flows around buried cables. Journal of the Geotechnical Engineering Division, ASCE. 107(11), 1461–1487.

Abuel-Naga HM Bergado DT and Bouazza A (2009) Thermomechanical model for saturated clays. Géotechnique. 59(3), 273–278.

Adam D and Markiewicz R (2009) Energy from earth-coupled structures, foundations, tunnels and sewers. Géotechnique. 59(3), 229–236.

Alsherif NA and McCartney JS (2014a) Effective stress in unsaturated silt under low degrees of saturation. Vadose Zone Journal. 13(5), 1-13. doi:10.2136/vzj2013.06.0109.

Alsherif NA and McCartney JS (2014b) Nonisothermal shear strength of compacted silt at residual saturation. Proceedings of GeoCongress 2014. Atlanta, GA. Feb. 23-26, 2014. 2745-2754.

ASTM D2435 (2011) Standard test methods for one-dimensional consolidation properties of soils using incremental loading. ASTM International, West Conshohocken, PA.

Baldi G Hueckel T and Pelegrini R (1988) Thermal volume changes of the mineral-water system in low-porosity clay soils. Canadian Geotechnical Journal. 25(4), 807-825.

Belanteur N Tacherifet S and Pakzad M (1997) Étude des comportements mécanique, thermo-mécanique et hydro-mécanique des argiles gonflantes et non gonflantes fortement compactées. Revue Française de Géotechnique 78, 31-50.

Bishop A W (1959) The principle of effective stress. Teknisk Ukeblad I Samarbeide Med Teknikk, Oslo, Norway. 106(39), 859–863.

Bourne-Webb PJ Amatya B and Soga K (2009) Energy pile test at Lambeth College, London: Geotechnical and thermodynamic aspects of pile response to heat cycles. Géotechnique. 59(3), 237–248.

Brandl H (2006) Energy foundations and other thermo-active ground structures. Géotechnique. 56(2), 81-122.

Brandon TL Mitchell JK and Cameron JT (1989) Thermal instability in buried cable backfills. Journal of Geotechnical Engineering, 115(1), 38-55.

Cekerevac C and Laloui L (2004) Experimental study of thermal effects on the mechanical behaviour of a clay. International Journal of Numerical and Analytical Methods in Geomechanics. 28(3), 209–228.

Coccia CJR and McCartney JS (2012) A thermo-hydro-mechanical true triaxial cell for evaluation of the impact of anisotropy on thermally induced volume changes in soils. ASTM Geotechnical Testing Journal. 35(2), 227-237.

Delage P Sultan N and Cui YJ (2000) On the thermal consolidation of boom clay. Canadian Geotechnical Journal. 37(2), 343-354.

Delage P Cui YJ and Sultan N (2004) On the thermal behaviour of Boom clay. Proceedings Eurosafe 2004 Conference, Berlin. 1-8. (CD-ROM).

Francois B Salager S and El Youssoufi MS (2005) Compression tests on a sandy silt at different suction and temperature levels. Computer Applications in Geotechnical Engineering. ASCE Geotechnical Special Publication 157. 1-10. (CD-ROM).

Gens A Garcia-Molina AJ and Olivella S (1998) Analysis of a full scale in situ test simulating repository conditions. International Journal of Numerical and Analytical Methods in Geomechanics. 22, 515–548.

Ghembaza MS Taïbi S and Fleureau JM (2007b) Some aspects of the effect of the temperature on the behaviour of unsaturated sandy clay. Experimental Unsaturated Soil Mechanics. Schanz, Tom (Ed.) Springer, Vienna. 243-250.

Graham J Wiebe B, Tang X and Onofrei C (1995) Strength and stiffness of unsaturated sand–bentonite 'buffer'. Proceedings of the 1st International Conference on Unsaturated Soils, Paris. Edited by E.E. Alonso and P. Delage. A.A. Balkema, Rotterdam. 89–94

Grant SA and Salehzadeh A (1996) Calculations of temperature- effects on wetting coefficients of porous solids and their capillary pressure functions. Water Resources Research. 32(2), 261–279.

Houston SL Houston WN and Williams ND (1985) Thermo-mechanical behavior of seafloor sediments. Journal of Geotechnical Engineering. 111(12), 1249-1263.

Hueckel T and Baldi M (1990) Thermoplasticity of saturated clays: experimental constitutive study. Journal of Geotechnical Engineering, 116(12), 1778–1796.

Hueckel T François B and Laloui L (2009) Explaining thermal failure in saturated clays. Géotechnique. 59(3), 197–212.

Imbert C Olchitzky E and Lassabatere T (2005) Evaluation of a thermal criterion for an engineered barrier system. Engineering Geology. 81(3), 269–283

Kanno T Fujita T and Ishikawa H (1999) Coupled thermo-hydro-mechanical modelling of bentonite buffer material. International Journal of Numerical and Analytical Methods in Geomechanics. 23(12), 1281–1307.

Khalili N and Khabbaz MH (1998) A unique relationship for χ for the determination of the shear strength of unsaturated soils. Géotechnique. 48(5), 681–687.

Laloui L Nuth M and Vulliet L (2006) Experimental and numerical investigations of the behaviour of a heat exchanger pile. International Journal of Numerical and Analytical Methods in Geomechanics. 30(8), 763-781.

Likos W and Lu N (2003) Automated humidity system for measuring total suction characteristics of clay. Geotechnical Testing Journal, 26(2), 179-190.

Lu N and Likos W (2006) Suction stress characteristic curve for unsaturated soil. Journal of Geotechnical Geoenvironmental Engineering. 132(2), 131–142.

Lu N Godt J and Wu D (2010) A closed-form equation for effective stress in unsaturated soil. Water Resources Research. 46(5), 1–14.

McCartney JS (2012) Issues involved in using temperature to improve the mechanical behavior of unsaturated soils. Unsaturated Soils: Theory and Practice 2011, Proc. 5th Asia-Pacific Unsaturated Soils Conference. Jotisankasa, Sawangsuriya, Soralump and Mairaing (Editors). Kasetsart University, Thailand. 509-514.

Murphy KD McCartney JS and Henry KH (2015) Thermo-mechanical response tests on energy foundations with different heat exchanger configurations. Acta Geotechnica. 10(2), 179-195.

Olchitzky E (2002) Couplage hydromécanique et perméabilité d'une argile gonflante non saturée sous sollicitations hydriques et thermiques. Courbe de sorption et perméabilité à l'eau. Ph.D. Thesis, École nationale des ponts et chaussées, Paris, France.

Ng CWW and Pang YW (2000) Experimental investigations of the soil-water characteristics of a volcanic soil. Canadian Geotechnical Journal. 37(6), 1252–1264.

Preene M and Powrie W (2009) Ground energy systems: from analysis to geotechnical design. Géotechnique. 59(3), 261-271.

Romero E, Gens A and Lloret A (2001) Temperature effects on the hydraulic behaviour of an unsaturated clay. Geotechnical and Geological Engineering. 19(3-4), 311-332.

Romero E, Gens A and Lloret A (2003) Suction effects on a compacted clay under non-isothermal conditions. Géotechnique. 53(1), 65-81.

Salager S El Youssoufi MS and Saix C (2007) Influence of temperature on the water retention curve of soils. Experimental Unsaturated Soil Mechanics. Schanz, Tom (Ed.) Springer, Vienna. Volume 112. 251-258.

Salager S François B and El Youssoufi MS (2008) Experimental investigations of temperature and suction effects on compressibility and pre-consolidation pressure of a sandy silt. Soils and Foundations. 48(4), 453-466.

She HY and Sleep BE (1998) The effect of temperature on capillary pressure-saturation relationships for air-water and perchloroethylene-water systems. Water Resources Research. 34(10), 2587–2597.

Stewart MA Coccia CJR and McCartney JS (2014) Issues in the implementation of sustainable heat exchange technologies in reinforced, unsaturated soil structures. Proceedings of GeoCongress 2014 (GSP 234), M. Abu-Farsakh and L. Hoyos, eds. ASCE. 4066-4075.

Sultan N, Delage P and Cui YJ (2002) Temperature effects on the volume change behavior of boom clay. Engineering Geology. 64(2-3), 135-145.

Tang AM and Cui YJ (2005) Controlling suction by the vapour equilibrium technique at different temperatures and its application in determining the water retention properties of MX80 clay. Canadian Geotechnical Journal. 42(1), 287-296.

Tang AM Cui YJ and Barnel N (2008) Thermo-mechanical behaviour of a compacted swelling clay. Géotechnique. 58(1), 45-54.

Uchaipichat A and Khalili N (2009) Experimental investigation of thermo-hydro-mechanical behaviour of an unsaturated silt. Géotechnique. 59(4), 339-353.

Uchaipichat A Khalili N and Zargarbashi S (2011) A temperature controlled triaxial apparatus for testing unsaturated soils. Geotechnical Testing Journal, 34(5), 424-432.

van Genuchten MT (1980) A closed form equation for predicting the hydraulic conductivity of unsaturated soils. Soil Science Society of America Journal. 44(5), 892-898.

Villar MV and Gomez R (2007) Retention curves of two bentonites at high temperature. Experimental Unsaturated Soil Mechanics. Schanz, Tom (Ed.) Springer, Vienna. 267-274.

Wiebe B Graham J Tang GXM and Dixon D (1998) Influence of pressure, saturation, and temperature on the behaviour of unsaturated sand-bentonite. Canadian Geotechnical Journal. 35(2), 194-205.

LIST OF TABLE AND FIGURE CAPTIONS

Table 1. Summary of the initial conditions from the compression triaxial tests on unsaturated specimens at ambient and elevated temperatures

Test path	**Initial Temp. at bottom T (°C)**	**Initial degree of sat. S_r**	**Initial Void ratio e_0**	**Average air pressure u_a (kPa)**	**Conf. stress at consol. σ_3 (kPa)**	**Axial stress at consol. σ_a (kPa)**	**Initial mean net stress p_{net} (kPa)**	**Rel. hum. at bottom R_h (%)**	**Suction ψ (MPa)**	**Temp. at bottom shearing T (°C)**
Amb.	22.7	0.41	0.68	20	100	200	113	30.5	162	22.7
	22.8	0.41	0.68	20	200	400	247	30.6	161	22.8
	23.8	0.41	0.68	20	300	600	380	29.8	165	23.8
Amb.	22.9	0.40	0.69	20	100	200	113	12.0	289	22.9
	23.2	0.42	0.66	20	200	400	247	11.8	292	23.2
	22.6	0.41	0.68	20	300	600	380	12.0	289	22.6
T-S	23.1	0.41	0.67	20	100	200	113	12.5	317	64.0
	23.0	0.41	0.67	20	200	400	247	12.5	317	64.0
	23.8	0.42	0.67	20	300	600	380	13.0	311	63.9
S-T	24.1	0.42	0.67	20	100	200	113	14.9	291	63.9
	23.5	0.41	0.68	20	200	400	247	15.0	290	63.9
	23.1	0.41	0.68	20	300	600	380	15.1	289	63.9
S-T Cycle	23.7	0.42	0.67	20	300	600	380	18.0	235	25.2

Table 2. Summary of the results from compression triaxial tests on unsaturated specimens at ambient and elevated temperatures

Test path	Suction ψ (MPa)	Temp. at bottom shearing T (°C)	Void ratio at shear e_s	Princ. stress diff. σ_1-σ_3 (kPa)	Exp. suction stress σ_s (kPa)	Initial shear stress q_0 (kPa)	Initial mean effective stress p'_0 (kPa)	Mean net stress at peak p_n (kPa)	Mean effective stress at peak p' (kPa)	Final void ratio e_f	Final degree of sat. S_r
Room	162	22.7	0.572	1965	202	100	128	735	937	0.576	0.10
	161	22.8	0.503	2679	202	200	261	1073	1275	0.507	0.11
	165	23.8	0.508	3364	202	300	390	1401	1603	0.513	0.12
Room	289	22.9	0.48	2392	263	100	128	877	1140	0.49	0.05
	292	23.2	0.49	3142	263	200	261	1227	1490	0.51	0.08
	289	22.6	0.39	3563	263	300	390	1468	1731	0.40	0.06
T-S	317	64.0	0.56	2235	235	100	128	825	1060	0.56	0.06
	317	64.0	0.52	2986	235	200	261	1175	1410	0.53	0.06
	311	63.9	0.48	3408	235	300	390	1416	1651	0.49	0.06
S-T	291	63.9	0.53	2707	313	100	128	982	1295	0.54	0.04
	290	63.9	0.468	3480	313	200	261	1340	1653	0.469	0.03
	289	63.9	0.36	4135	313	300	390	1658	1971	0.37	0.04
S-T Cycle	235	25.2	0.39	3699	263	300	390	1513	1776	0.39	0.07

Alsherif and McCartney - Figure 01

Click here to download Figure: Alsherif and McCartney - Figure 01.tif

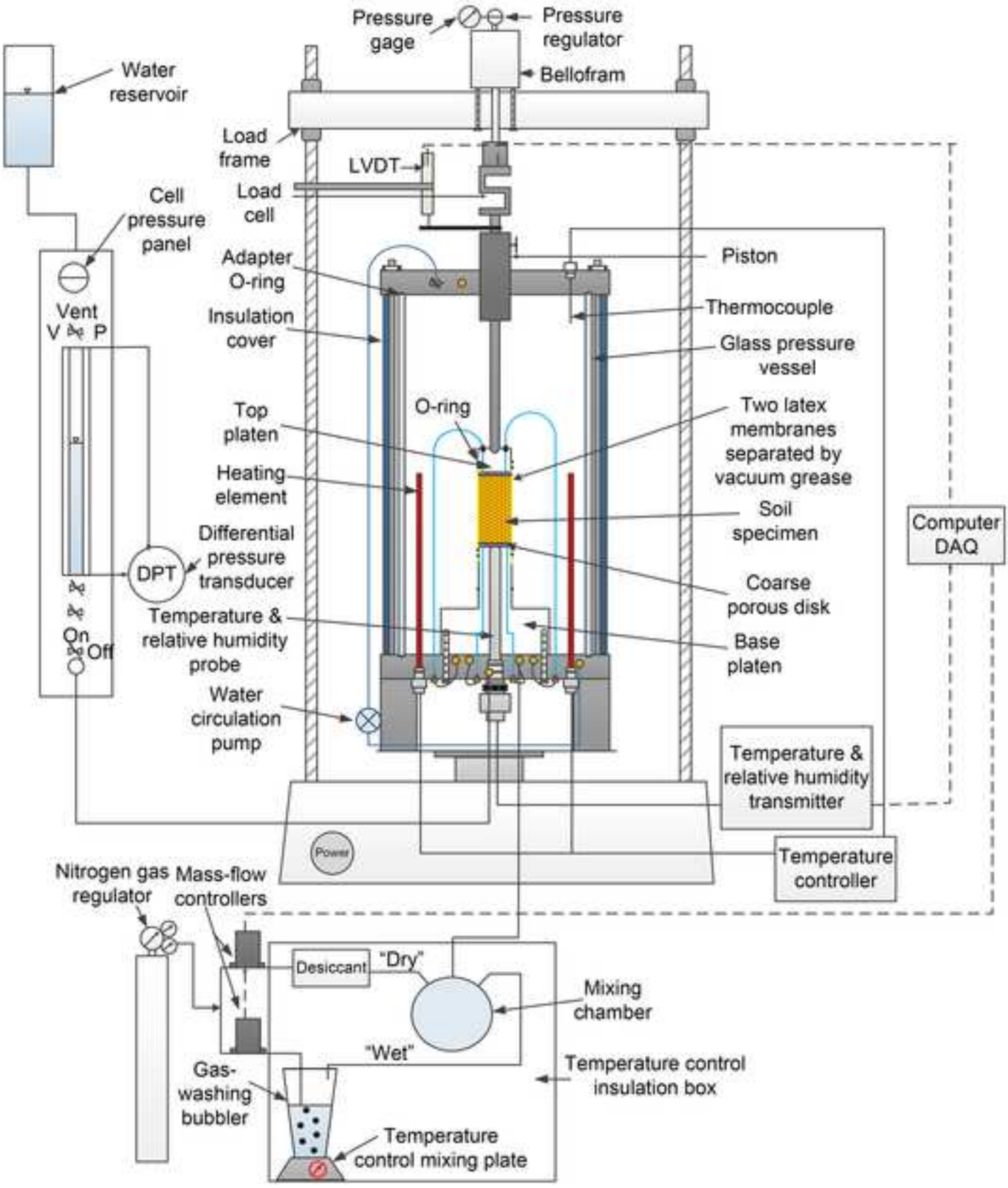

Alsherif and McCartney - Figure 03
Click here to download Figure: Alsherif and McCartney - Figure 03.tif

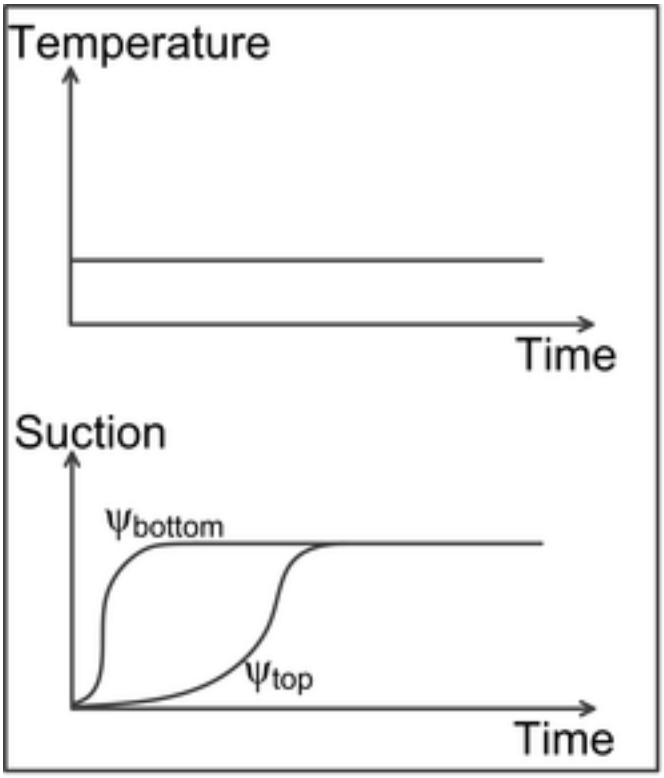

(a)

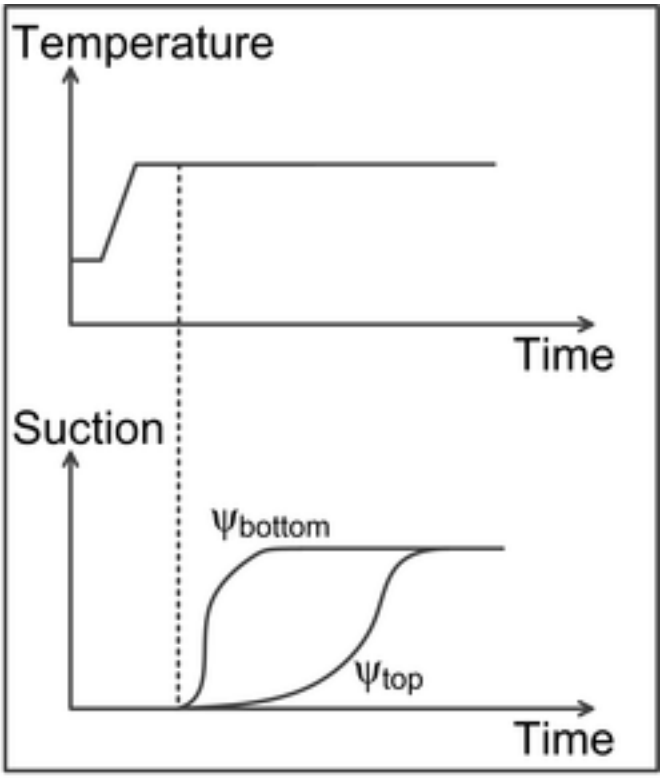

(b)

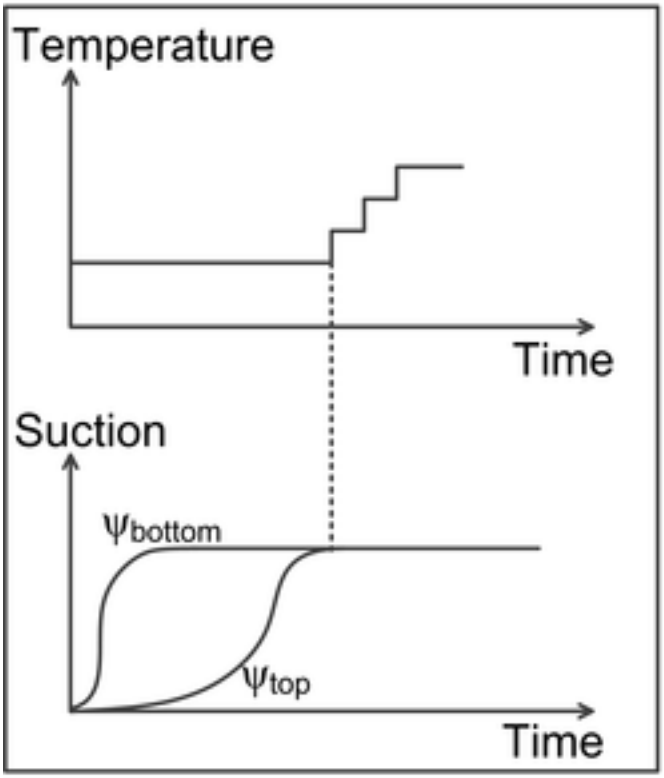

(c)

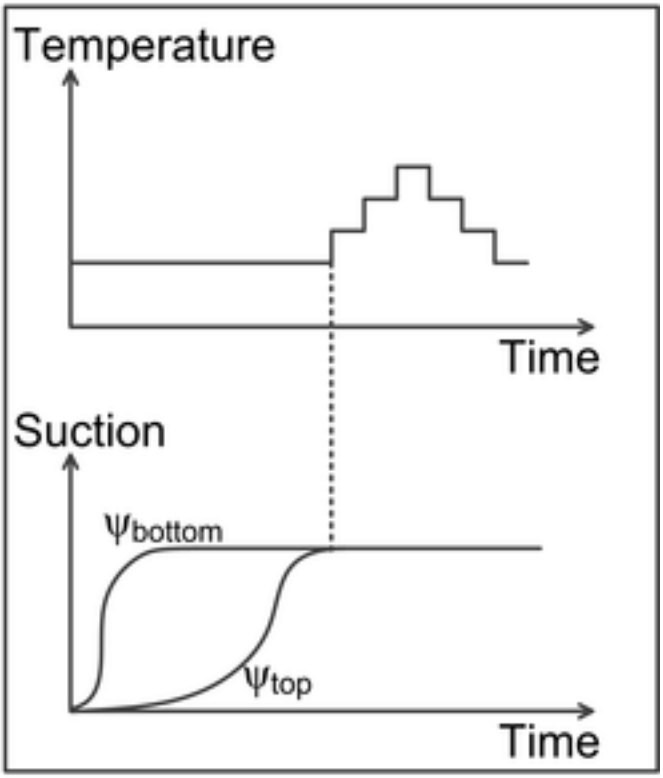

(d)

Alsherif and McCartney - Figures 02, 04 to 12
Click here to download Figure: Alsherif and McCartney - Figures 02, 04 to 12.xlsx

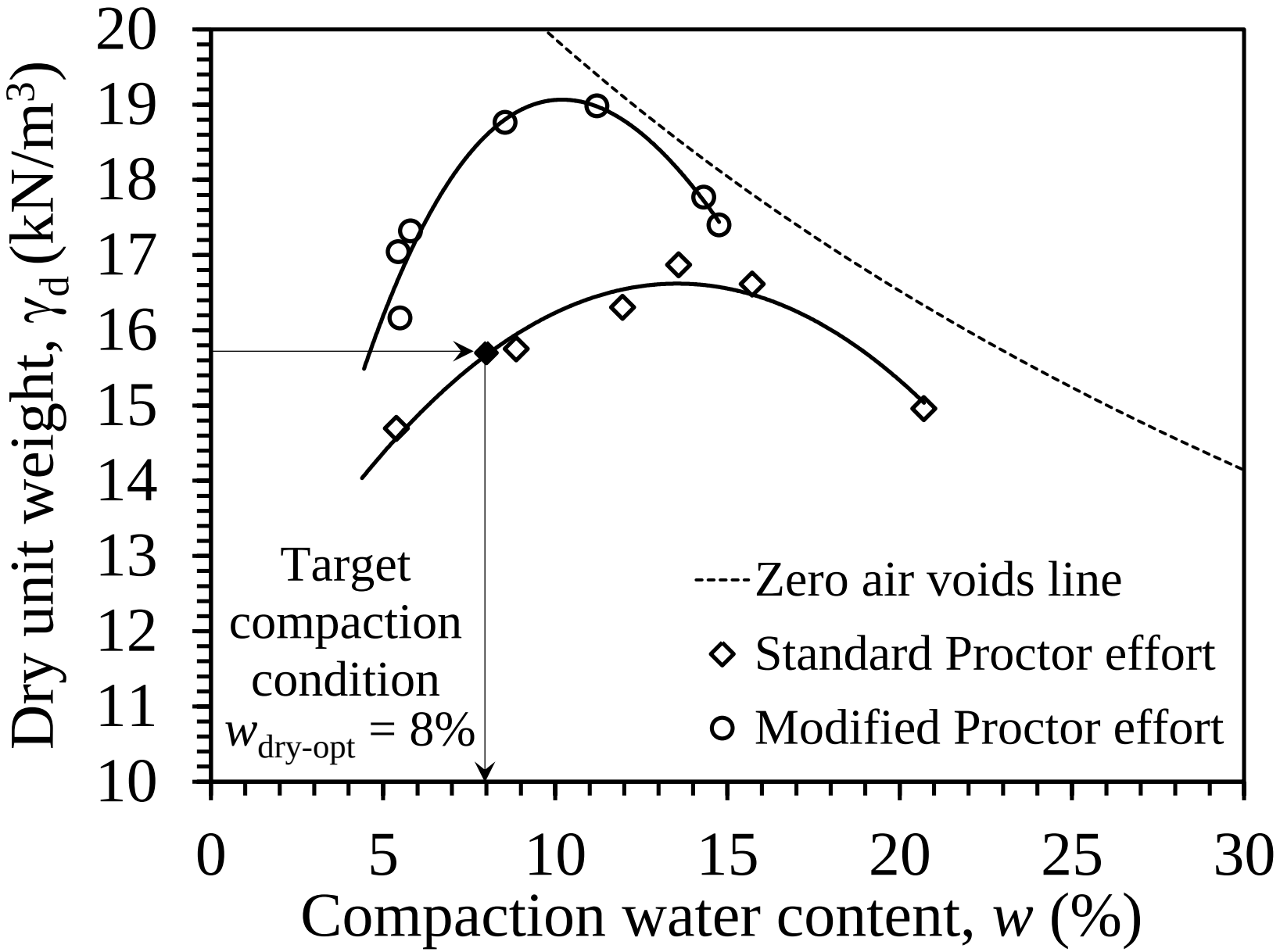

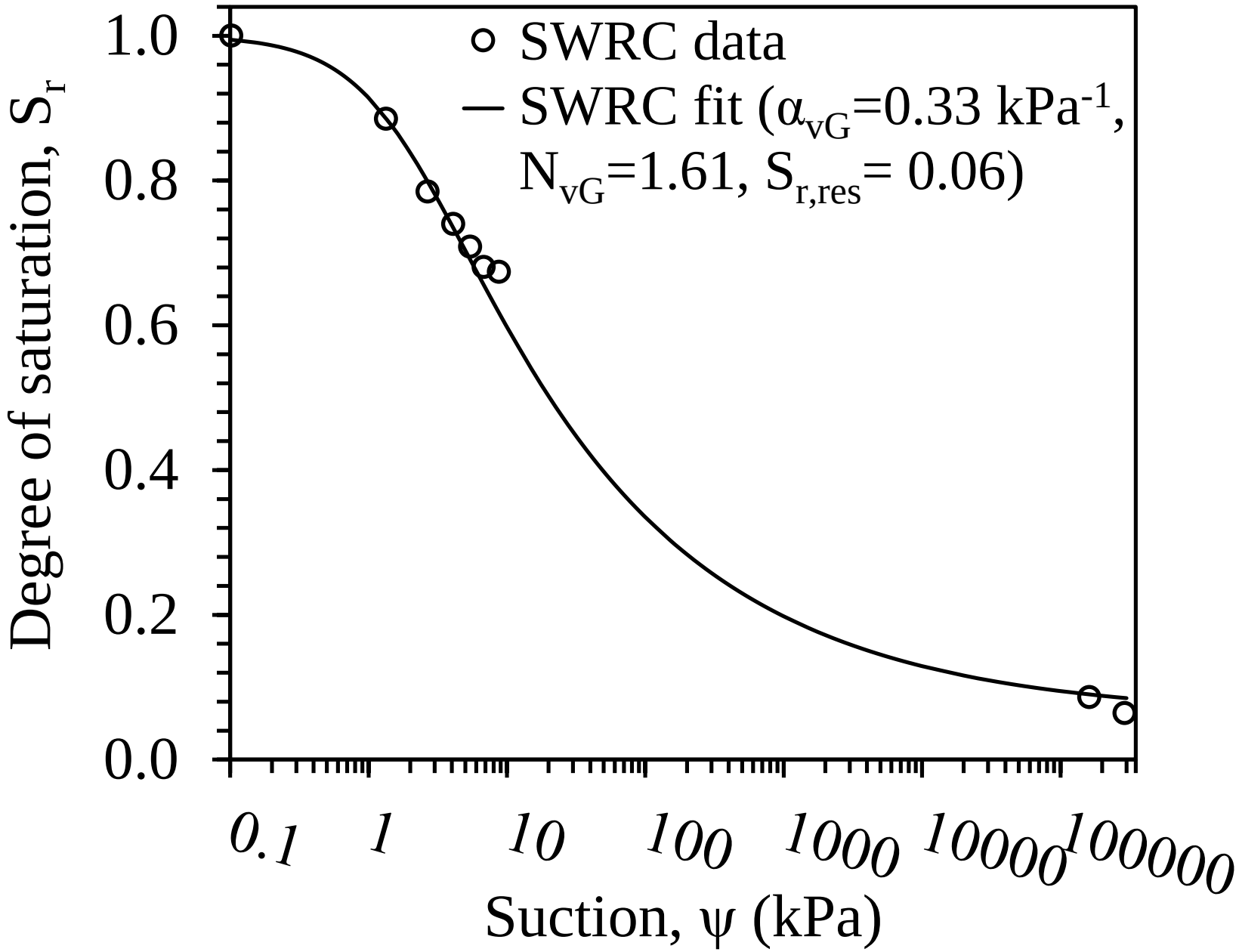
SWRC data
SWRC fit (α_{vG}=0.33 kPa^{-1}, N_{vG}=1.61, $S_{r,res}$= 0.06)
Degree of saturation, S_r
1.0
0.8
0.6
0.4
0.2
0.0
0.1
1
10
100
1000
10000
100000
Suction, ψ (kPa)

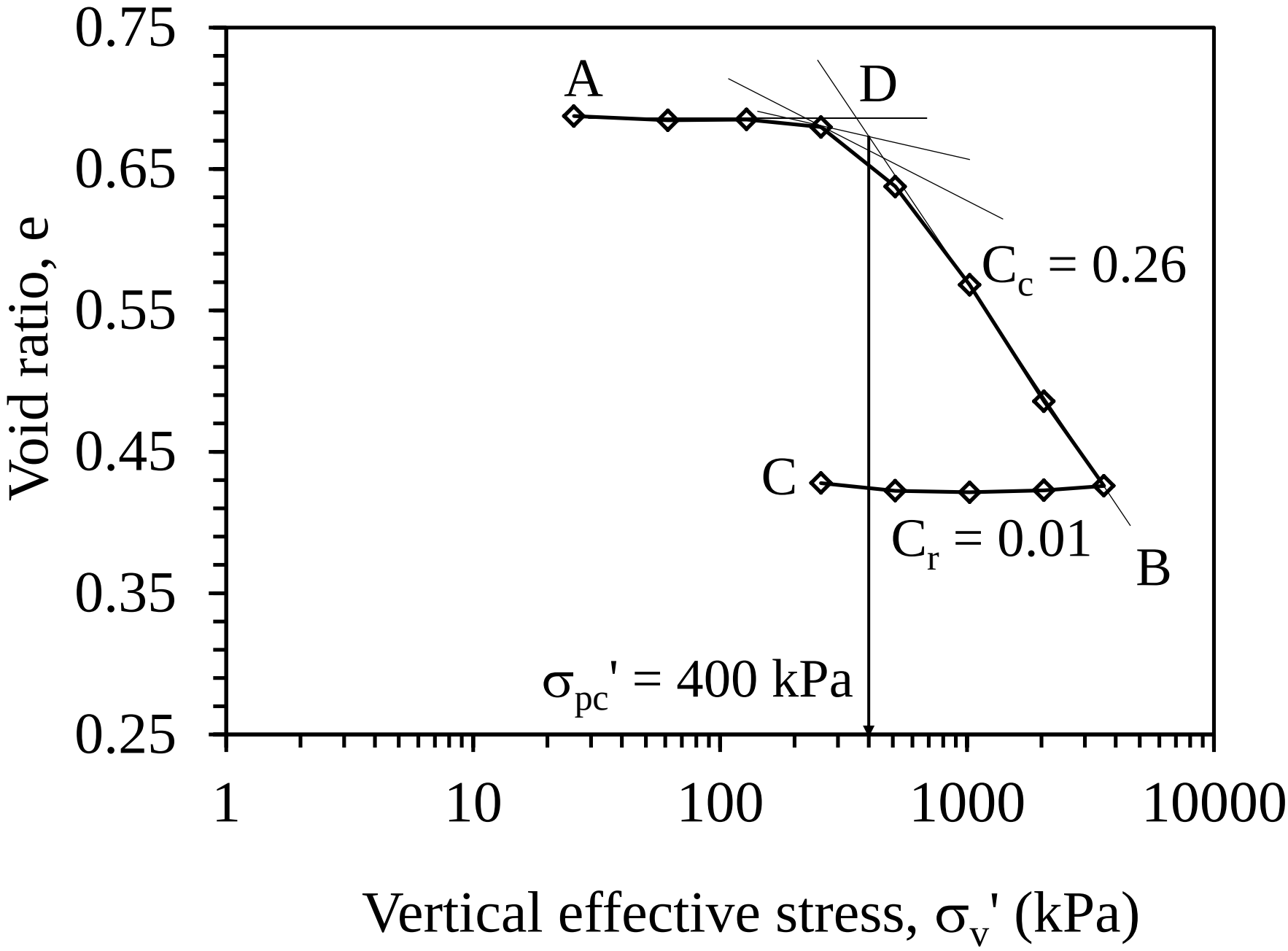
0.75
0.65
0.55
0.45
0.35
0.25
Void ratio, e
A
D
C
B
C_c = 0.26
C_r = 0.01
σ_{pc}' = 400 kPa
1
10
100
1000
10000
Vertical effective stress, σ_v' (kPa)

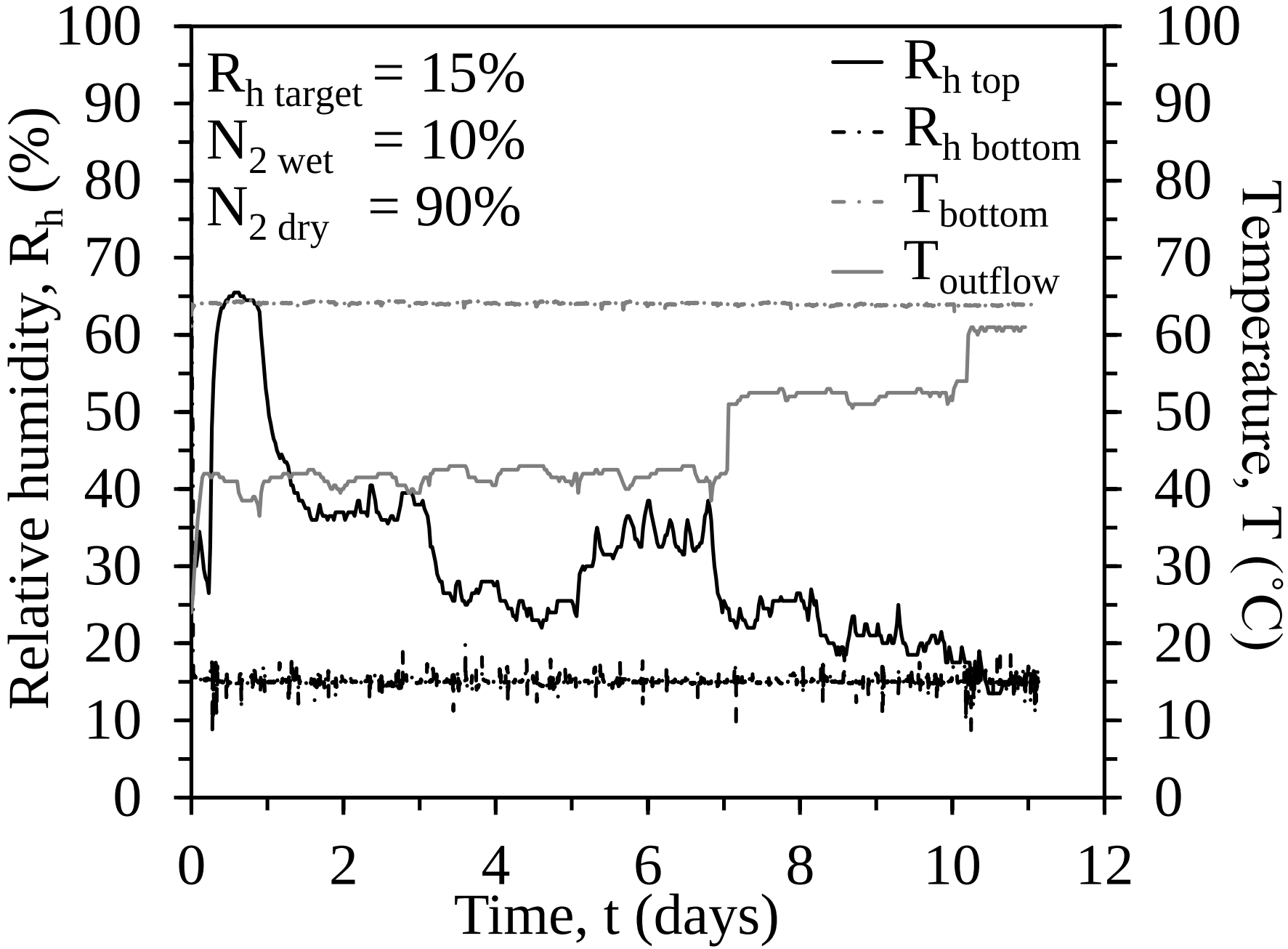
$R_{h\ target}$ = 15%
$N_{2\ wet}$ = 10%
$N_{2\ dry}$ = 90%
$R_{h\ top}$
$R_{h\ bottom}$
T_{bottom}
$T_{outflow}$
Relative humidity, R_h (%)
Temperature, T (°C)
Time, t (days)
0
10
20
30
40
50
60
70
80
90
100
0
2
4
6
8
10
12

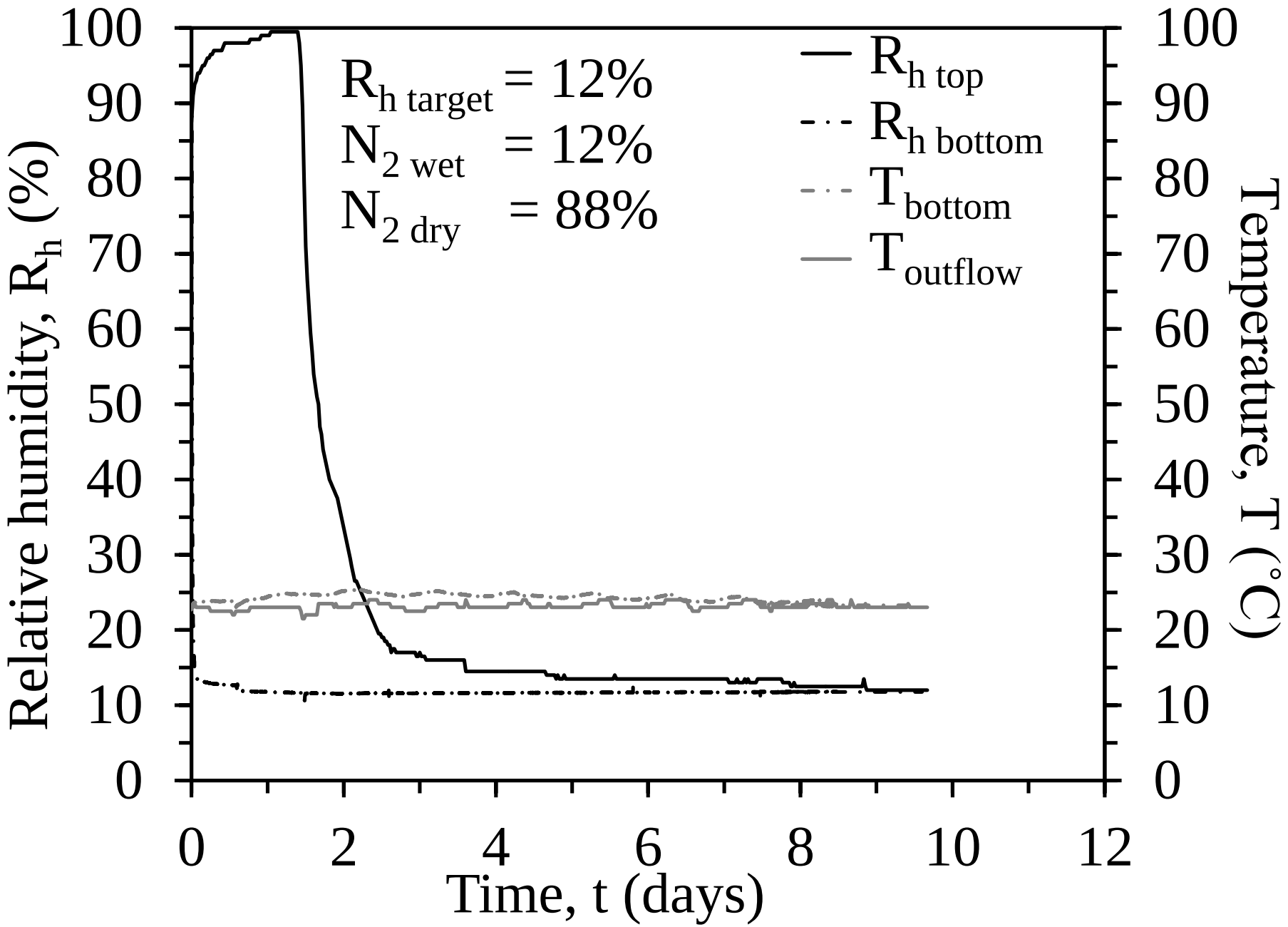
100
90
80
70
60
50
40
30
20
10
0
Relative humidity, R_h (%)
$R_{h\ target}$ = 12%
$N_{2\ wet}$ = 12%
$N_{2\ dry}$ = 88%
$R_{h\ top}$
$R_{h\ bottom}$
T_{bottom}
$T_{outflow}$
Temperature, T (°C)
0
2
4
6
8
10
12
Time, t (days)

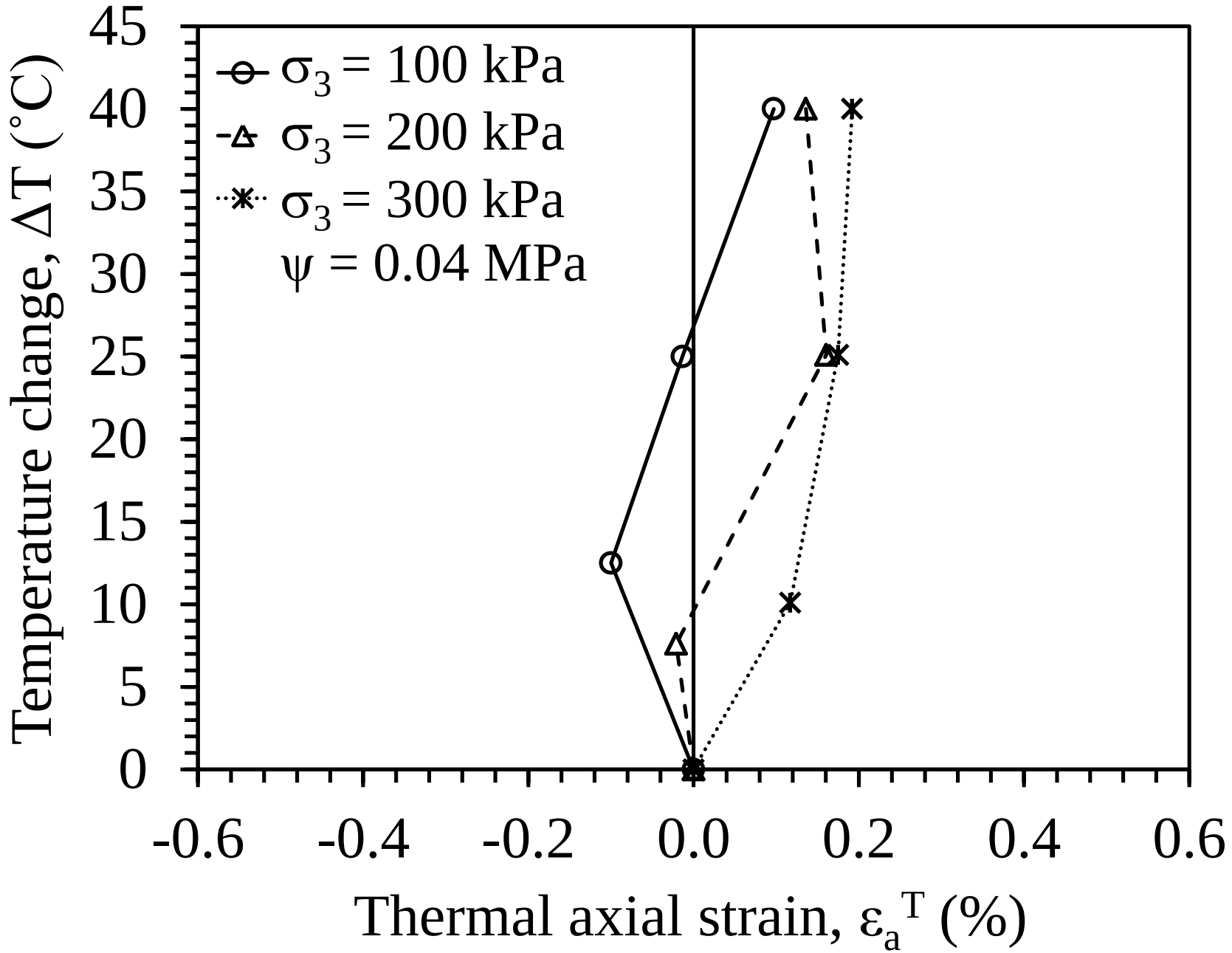
45
40
35
30
25
20
15
10
5
0
Temperature change, ΔT (°C)
σ3 = 100 kPa
σ3 = 200 kPa
σ3 = 300 kPa
ψ = 0.04 MPa
-0.6
-0.4
-0.2
0.0
0.2
0.4
0.6
Thermal axial strain, εa T (%)

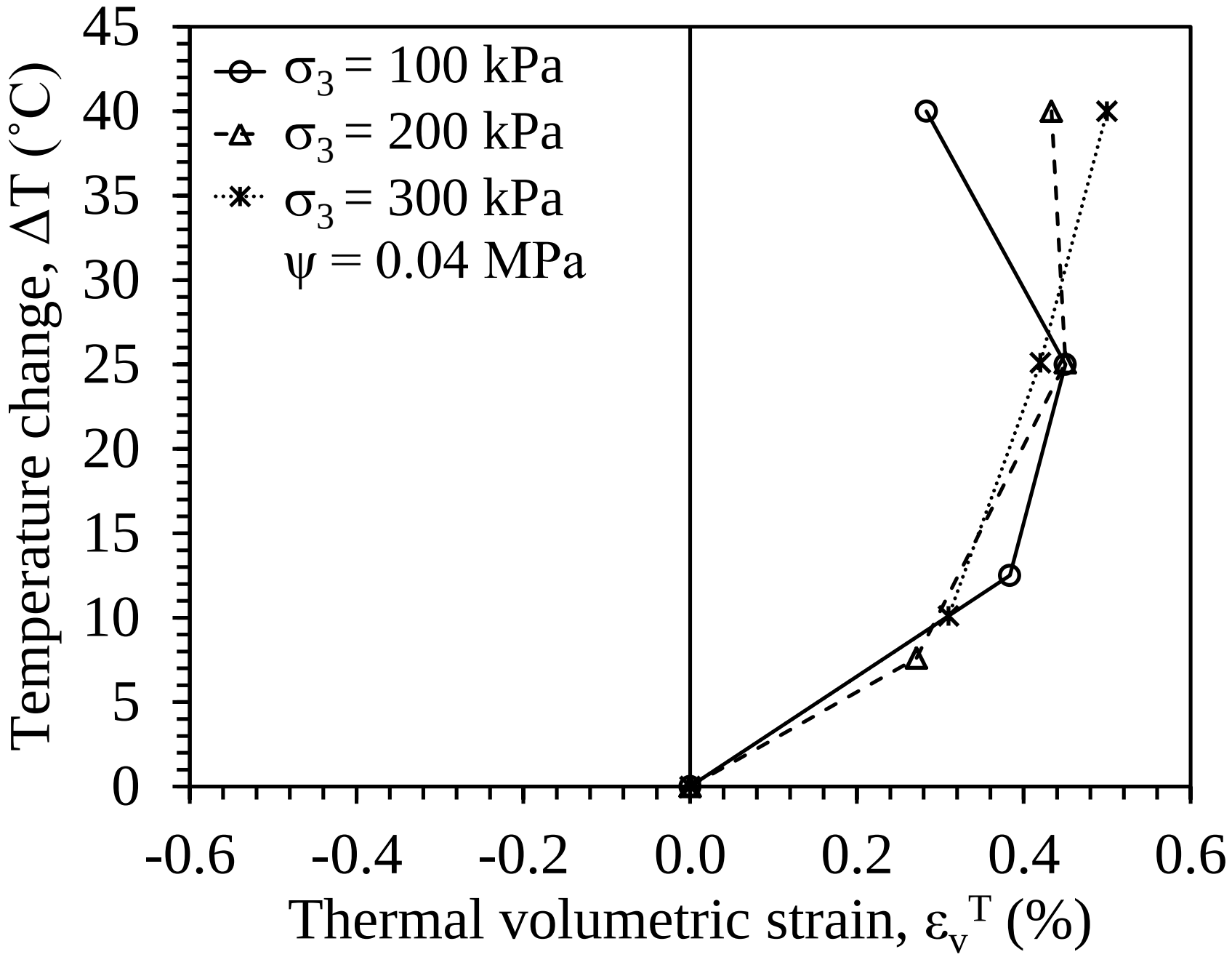
σ3 = 100 kPa
σ3 = 200 kPa
σ3 = 300 kPa
ψ = 0.04 MPa
Temperature change, ΔT (°C)
45
40
35
30
25
20
15
10
5
0
-0.6
-0.4
-0.2
0.0
0.2
0.4
0.6
Thermal volumetric strain, εv T (%)

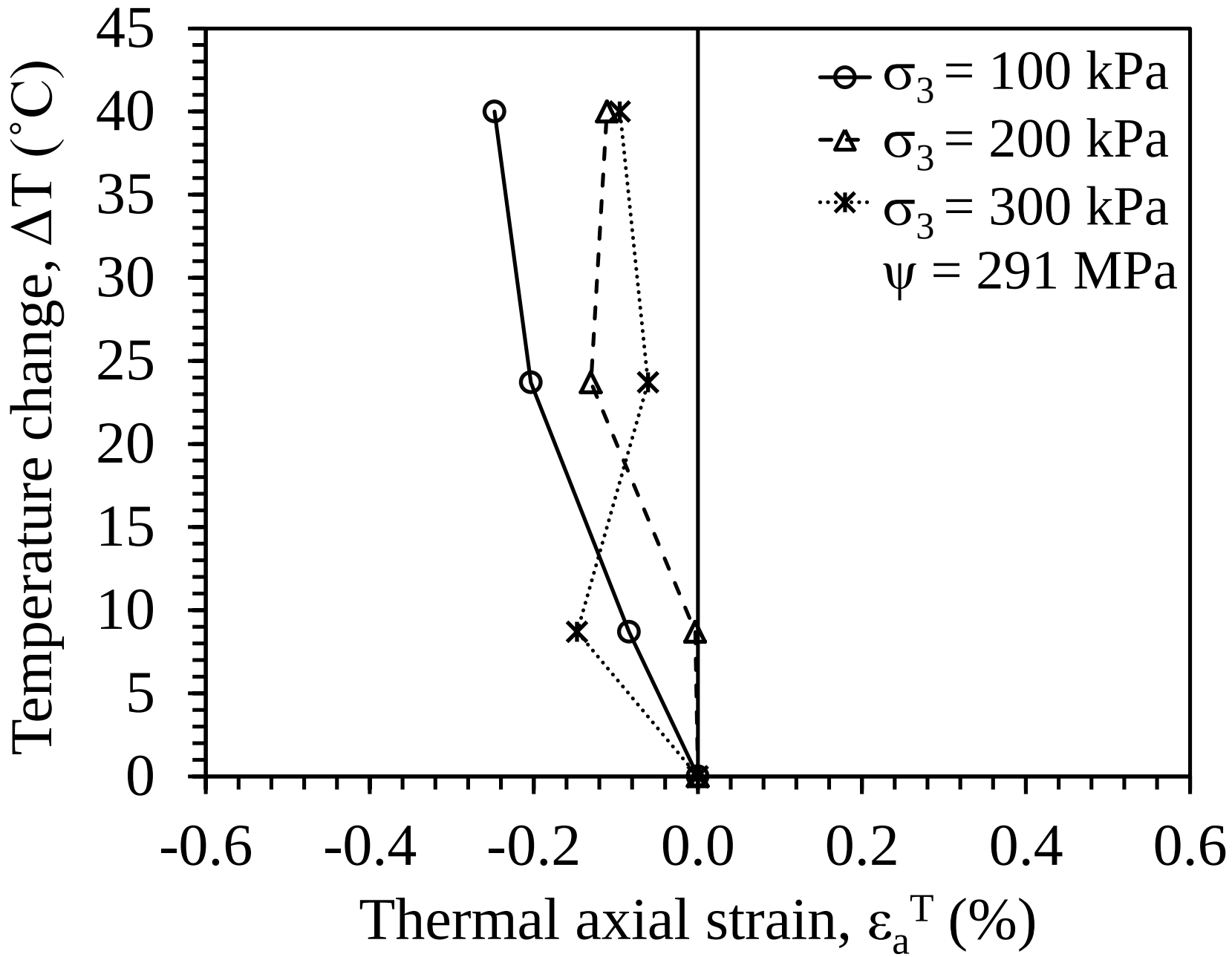
Temperature change, ΔT (°C)
45
40
35
30
25
20
15
10
5
0
-0.6
-0.4
-0.2
0.0
0.2
0.4
0.6
Thermal axial strain, ε_a^T (%)
σ_3 = 100 kPa
σ_3 = 200 kPa
σ_3 = 300 kPa
ψ = 291 MPa

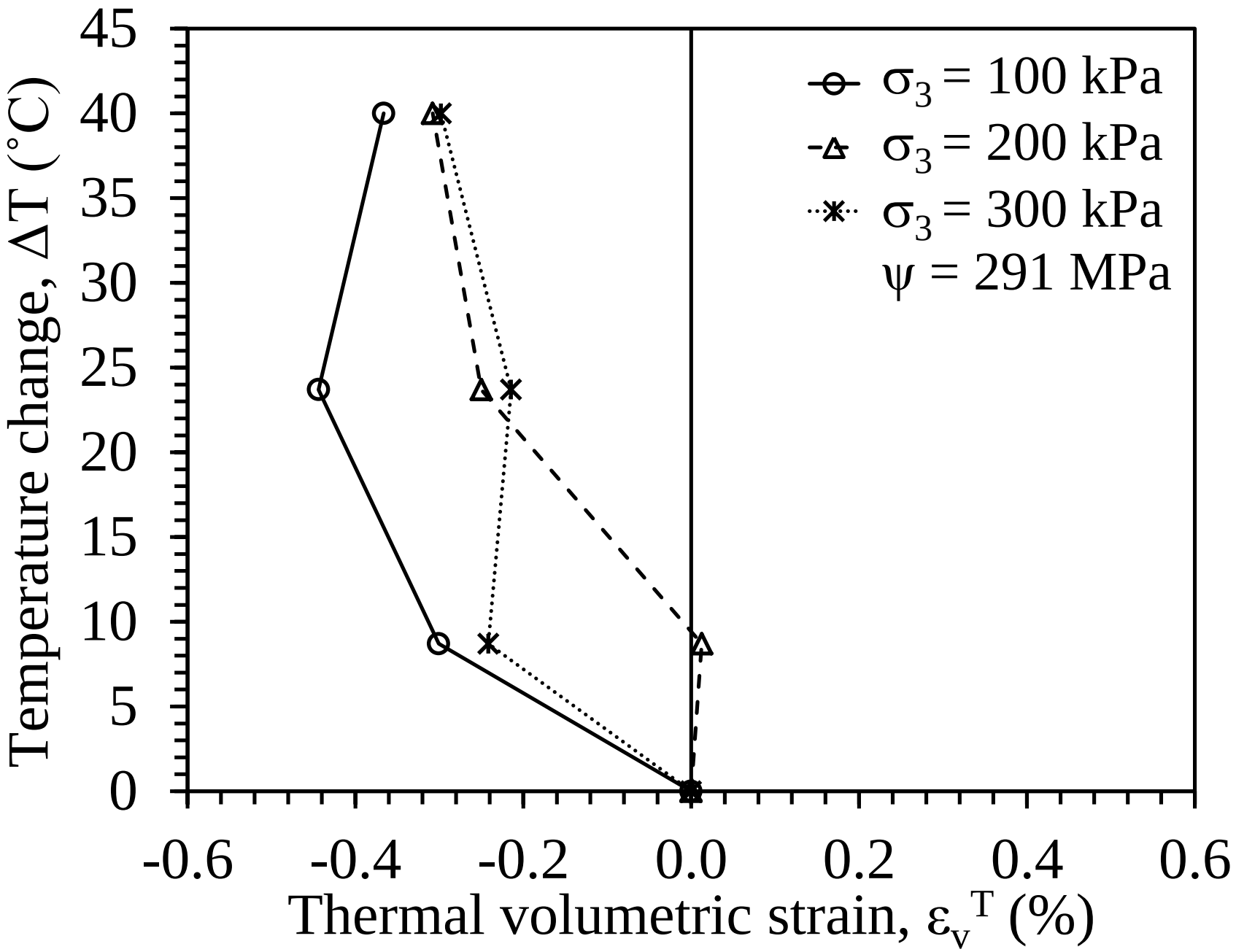
45
40
35
30
25
20
15
10
5
0
Temperature change, ΔT (°C)
-0.6
-0.4
-0.2
0.0
0.2
0.4
0.6
Thermal volumetric strain, εv T (%)
σ3 = 100 kPa
σ3 = 200 kPa
σ3 = 300 kPa
ψ = 291 MPa

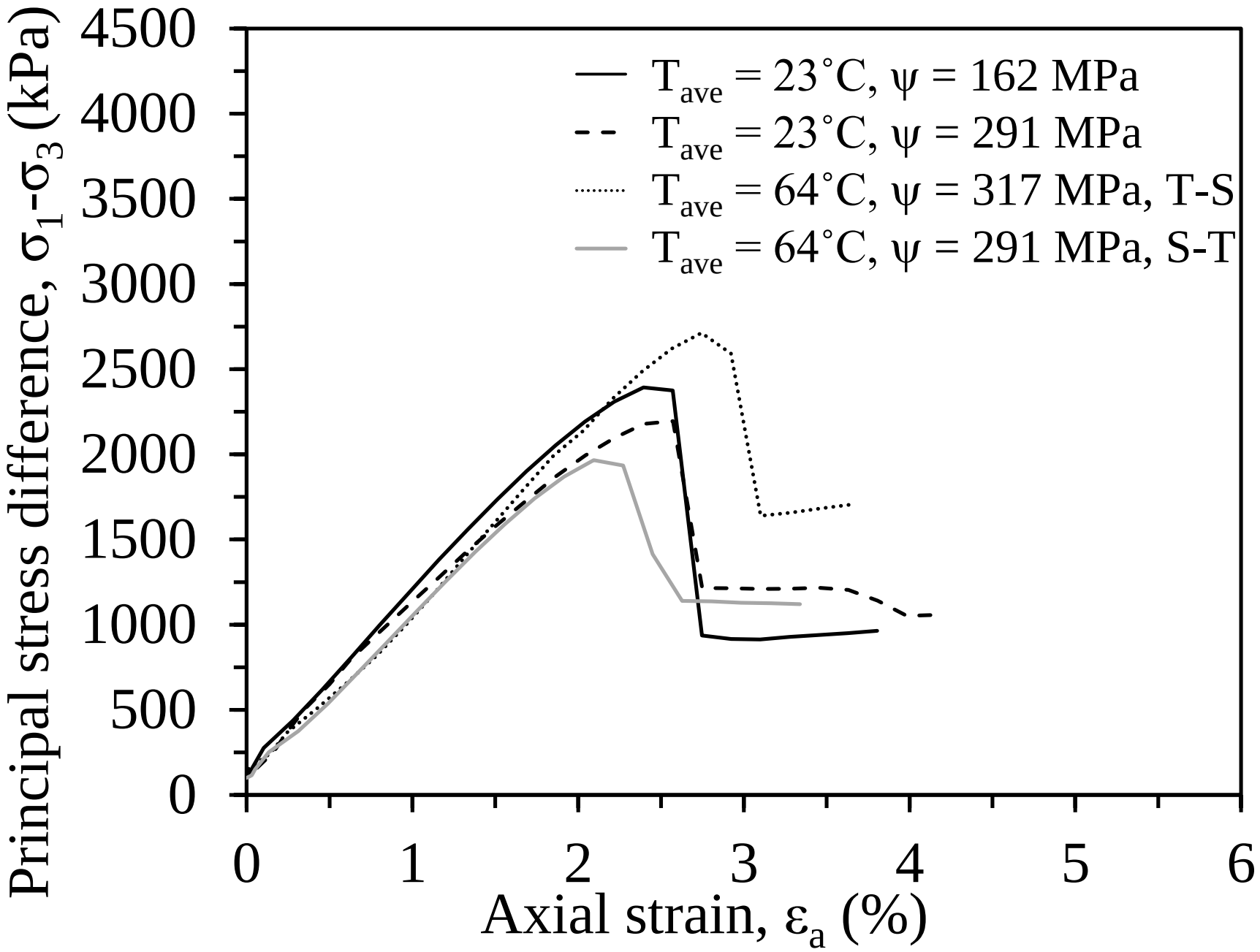
Principal stress difference, σ1-σ3 (kPa)
4500
4000
3500
3000
2500
2000
1500
1000
500
0
0
1
2
3
4
5
6
Axial strain, εa (%)
Tave = 23˚C, ψ = 162 MPa
Tave = 23˚C, ψ = 291 MPa
Tave = 64˚C, ψ = 317 MPa, T-S
Tave = 64˚C, ψ = 291 MPa, S-T

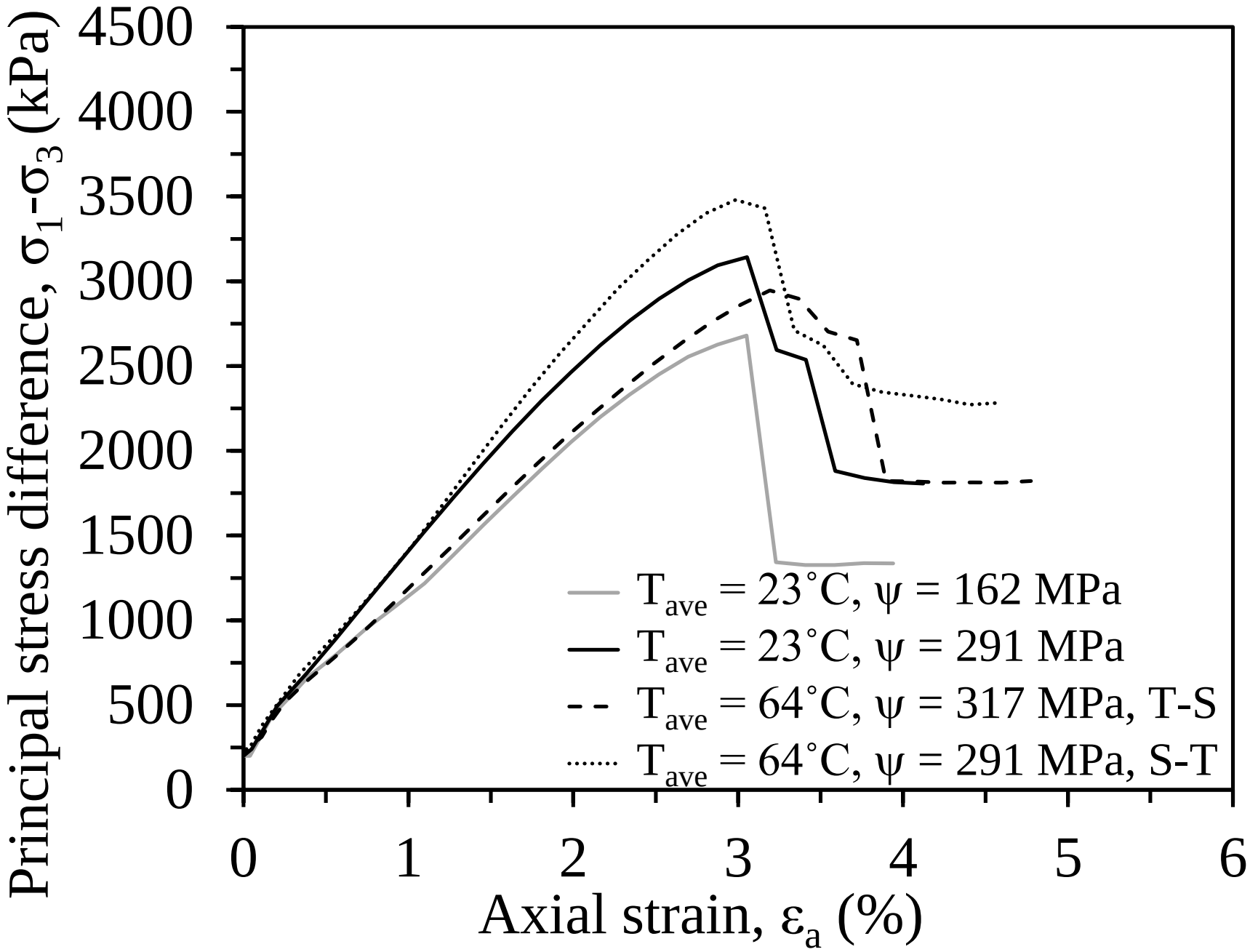
Principal stress difference, σ1-σ3 (kPa)
4500
4000
3500
3000
2500
2000
1500
1000
500
0
0
1
2
3
4
5
6
Axial strain, εa (%)
Tave = 23˚C, ψ = 162 MPa
Tave = 23˚C, ψ = 291 MPa
Tave = 64˚C, ψ = 317 MPa, T-S
Tave = 64˚C, ψ = 291 MPa, S-T

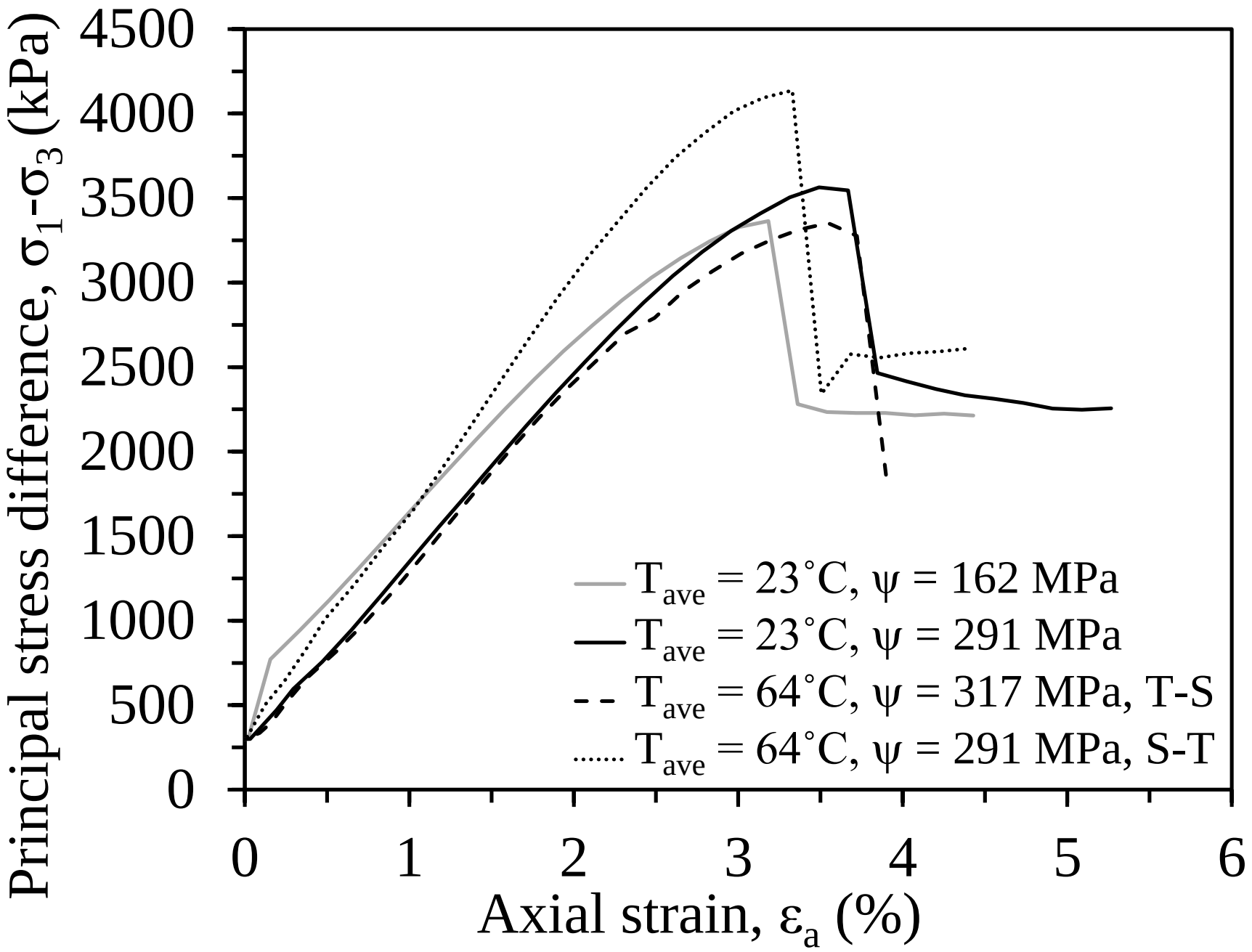
Principal stress difference, σ1-σ3 (kPa)
4500
4000
3500
3000
2500
2000
1500
1000
500
0
0
1
2
3
4
5
6
Axial strain, εa (%)
Tave = 23˚C, ψ = 162 MPa
Tave = 23˚C, ψ = 291 MPa
Tave = 64˚C, ψ = 317 MPa, T-S
Tave = 64˚C, ψ = 291 MPa, S-T

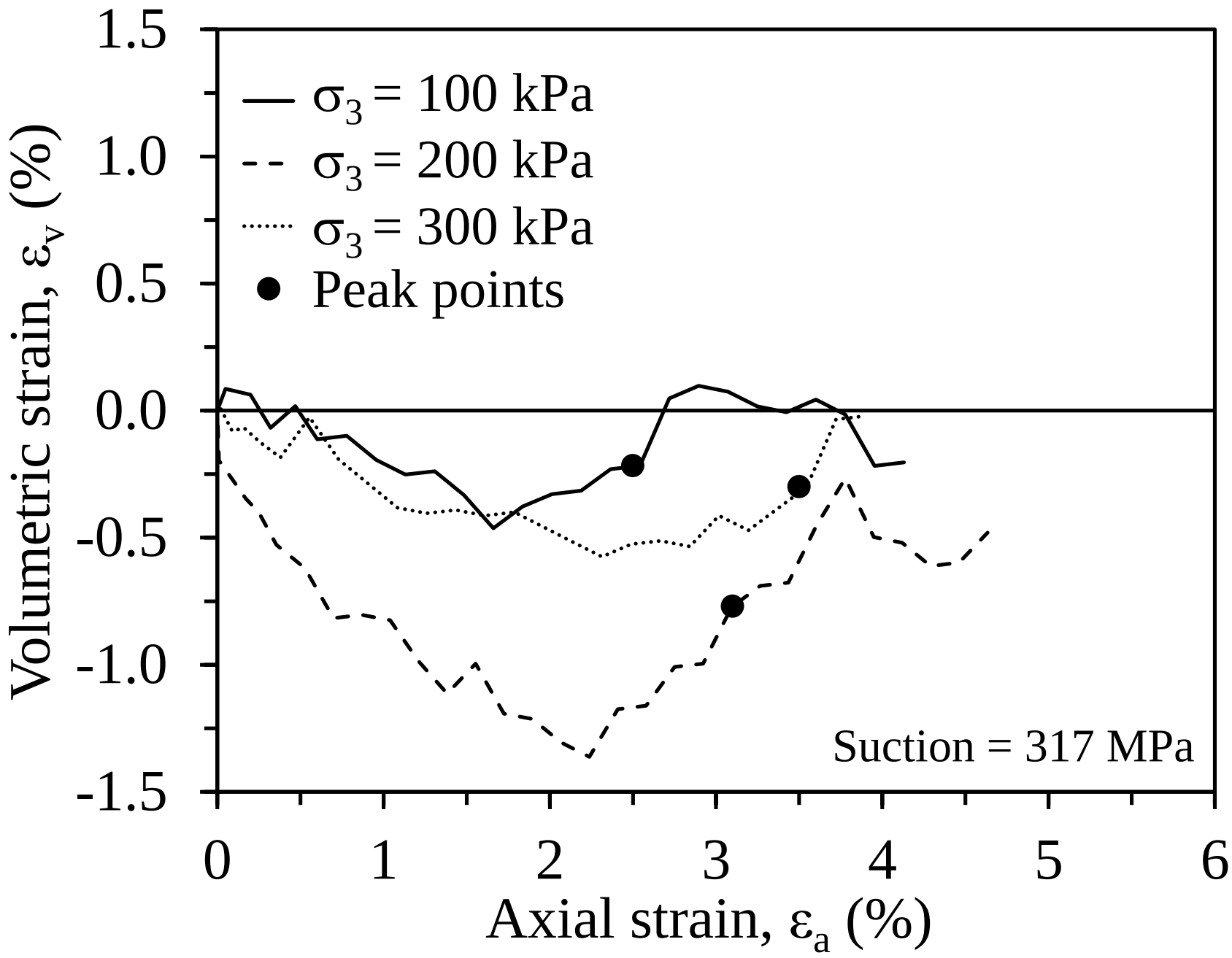
1.5
1.0
0.5
0.0
-0.5
-1.0
-1.5
Volumetric strain, εv (%)
σ3 = 100 kPa
σ3 = 200 kPa
σ3 = 300 kPa
Peak points
Suction = 317 MPa
0
1
2
3
4
5
6
Axial strain, εa (%)

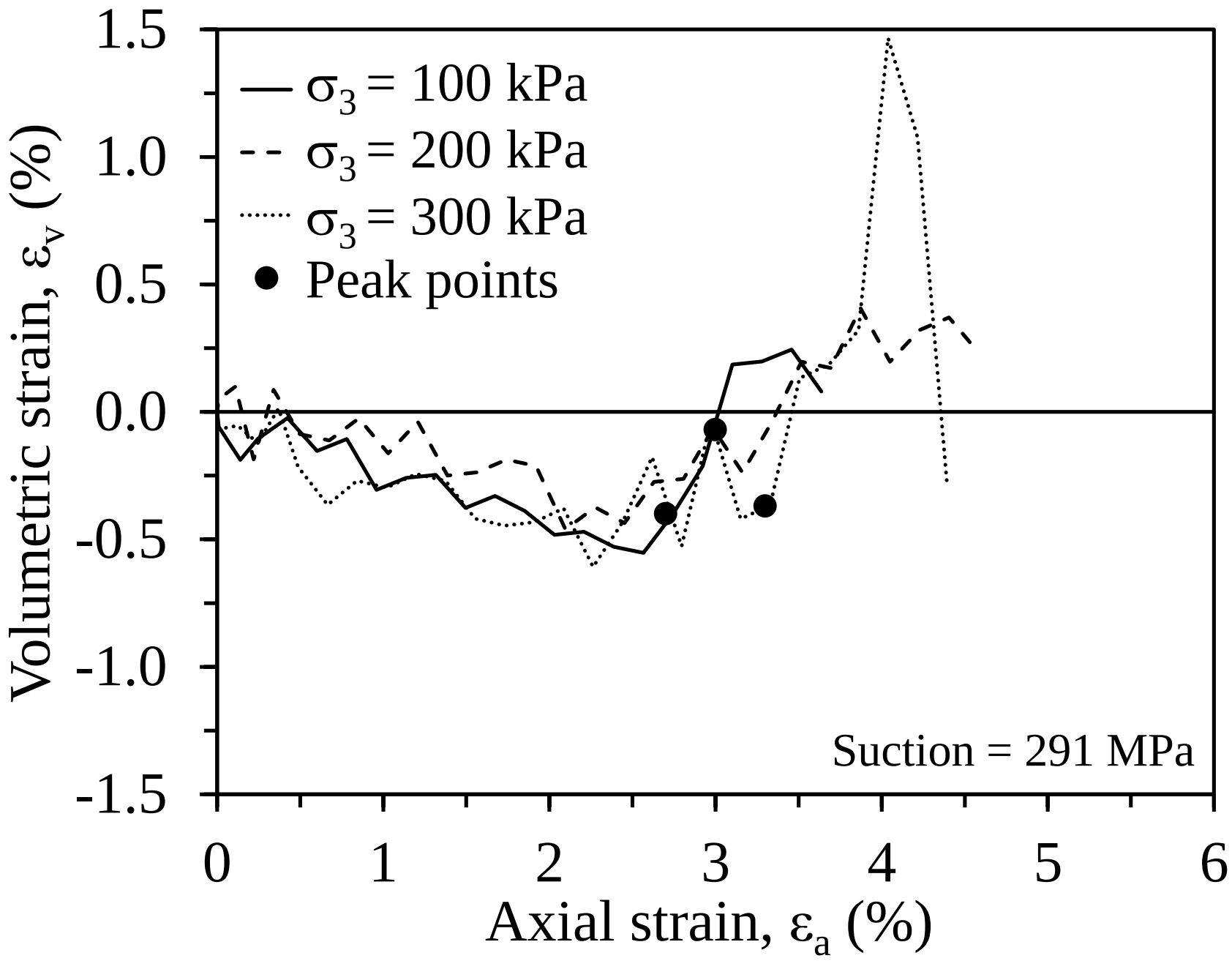
1.5
1.0
0.5
0.0
-0.5
-1.0
-1.5
0
1
2
3
4
5
6
Volumetric strain, εv (%)
Axial strain, εa (%)
σ3 = 100 kPa
σ3 = 200 kPa
σ3 = 300 kPa
Peak points
Suction = 291 MPa

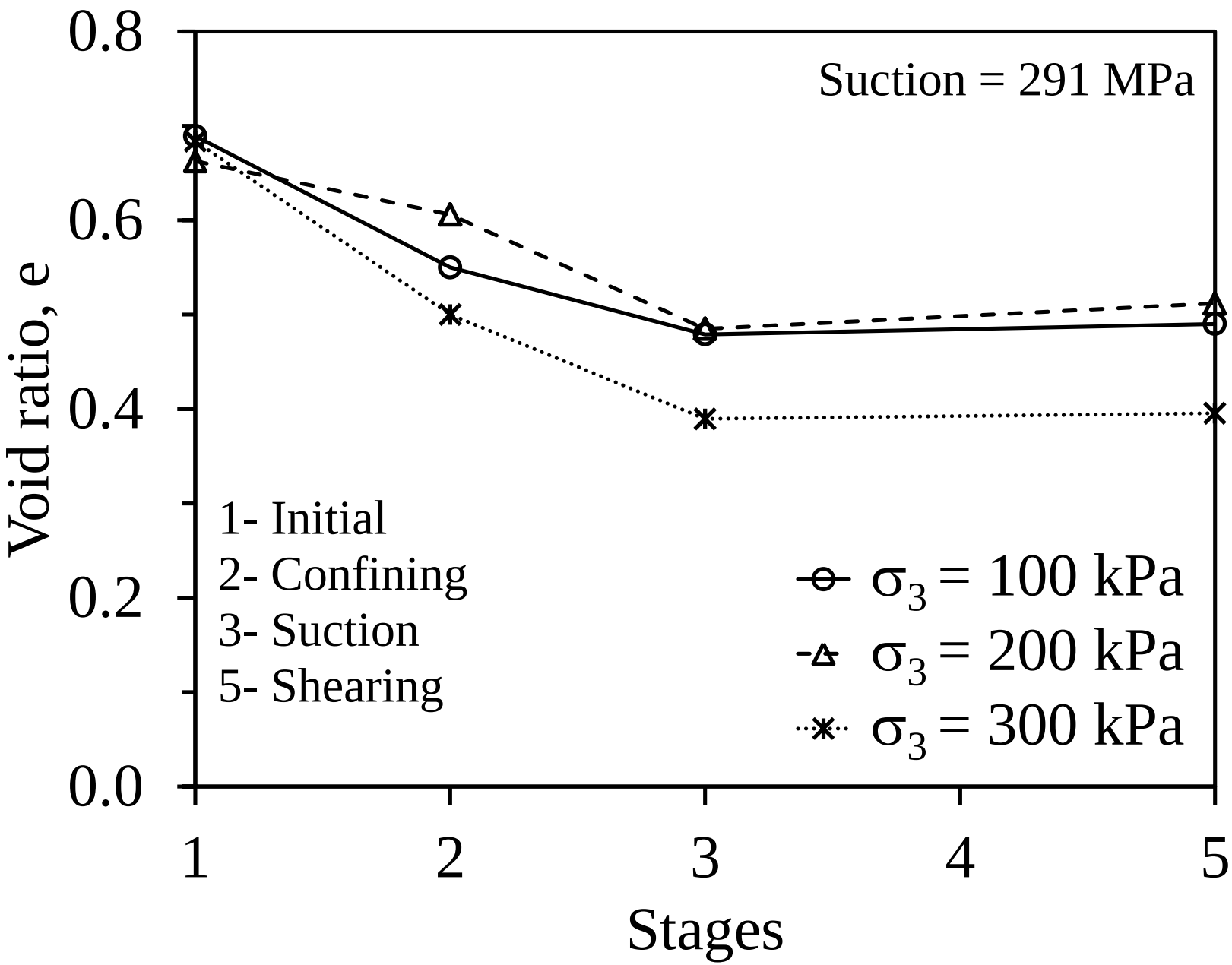
Suction = 291 MPa
Void ratio, e
0.8
0.6
0.4
0.2
0.0
1
2
3
4
5
Stages
1- Initial
2- Confining
3- Suction
5- Shearing
σ3 = 100 kPa
σ3 = 200 kPa
σ3 = 300 kPa

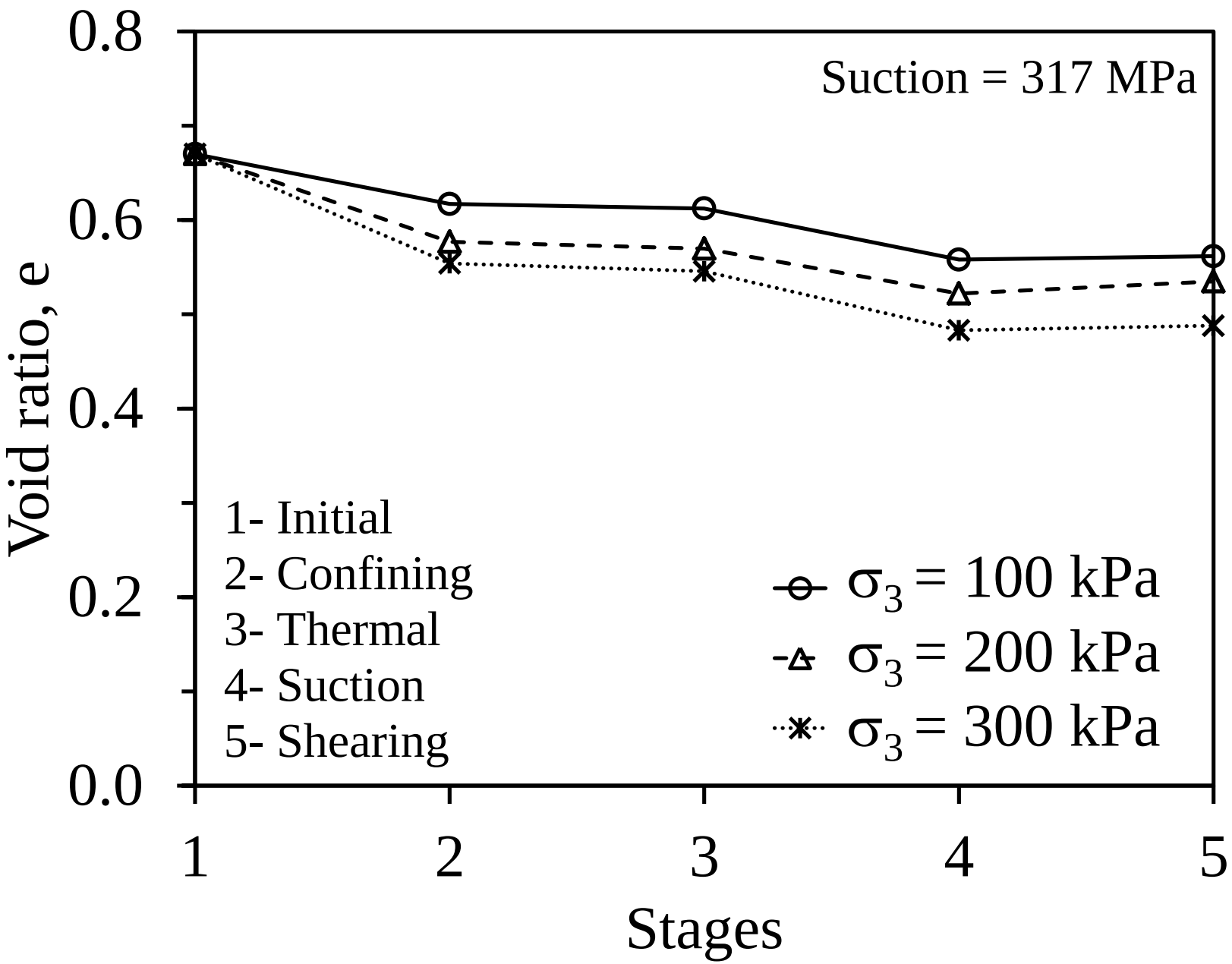
0.8
0.6
0.4
0.2
0.0
Void ratio, e
Suction = 317 MPa
1- Initial
2- Confining
3- Thermal
4- Suction
5- Shearing
σ3 = 100 kPa
σ3 = 200 kPa
σ3 = 300 kPa
1
2
3
4
5
Stages

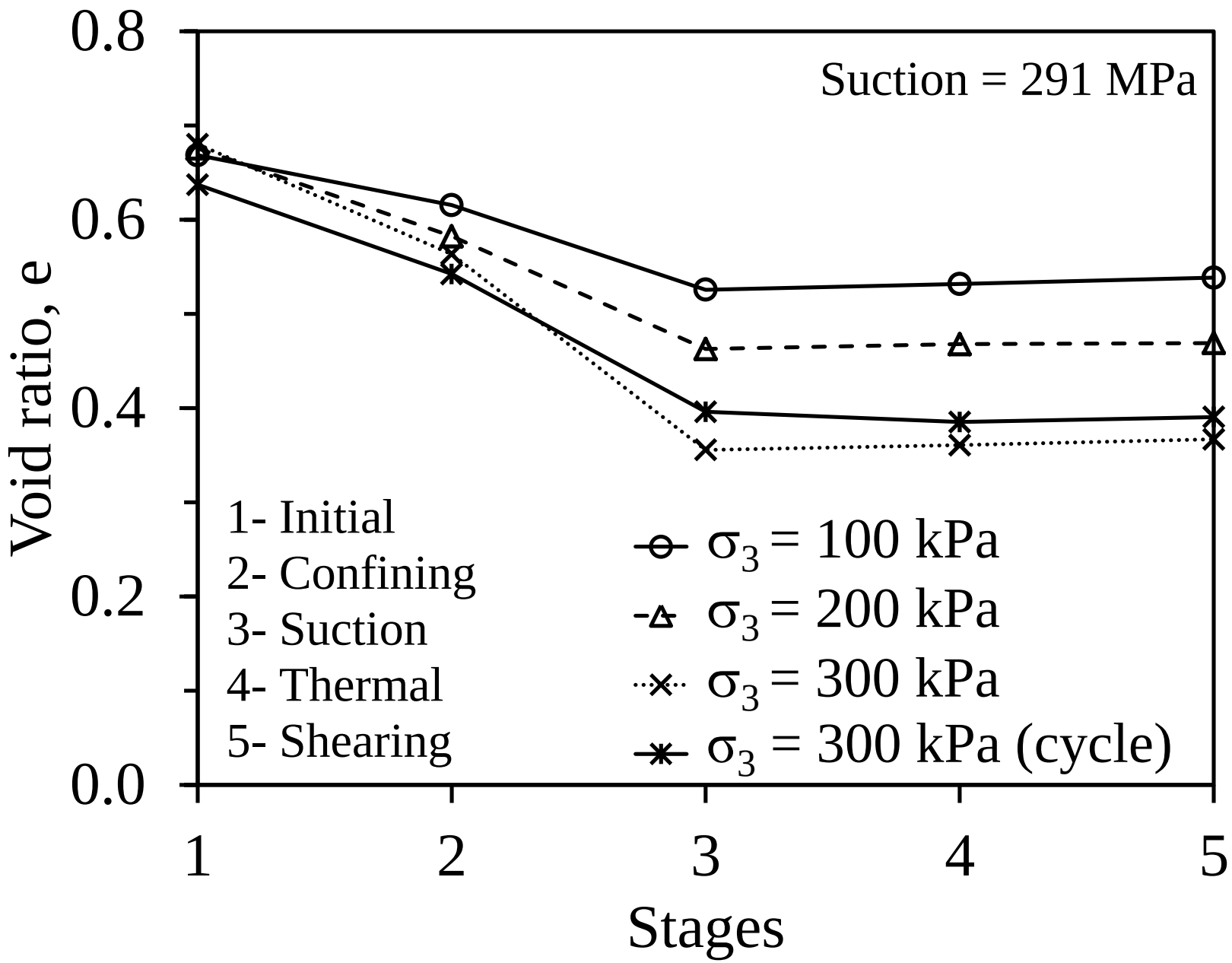
Suction = 291 MPa
Void ratio, e
0.8
0.6
0.4
0.2
0.0
1
2
3
4
5
Stages
1- Initial
2- Confining
3- Suction
4- Thermal
5- Shearing
σ3 = 100 kPa
σ3 = 200 kPa
σ3 = 300 kPa
σ3 = 300 kPa (cycle)

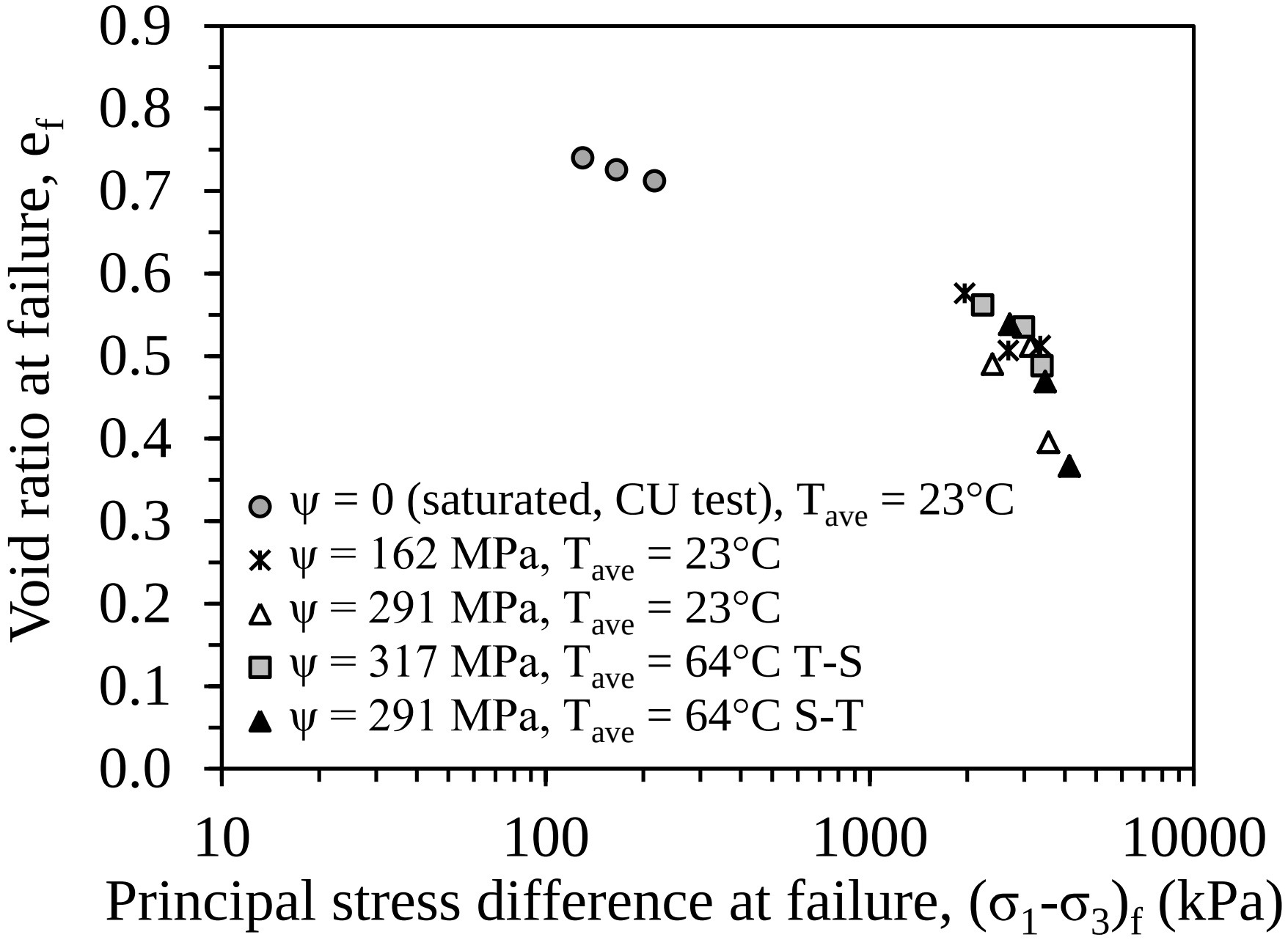
0.9
0.8
0.7
0.6
0.5
0.4
0.3
0.2
0.1
0.0
Void ratio at failure, e_f
ψ = 0 (saturated, CU test), T_{ave} = 23°C
ψ = 162 MPa, T_{ave} = 23°C
ψ = 291 MPa, T_{ave} = 23°C
ψ = 317 MPa, T_{ave} = 64°C T-S
ψ = 291 MPa, T_{ave} = 64°C S-T
10
100
1000
10000
Principal stress difference at failure, $(\sigma_1-\sigma_3)_f$ (kPa)

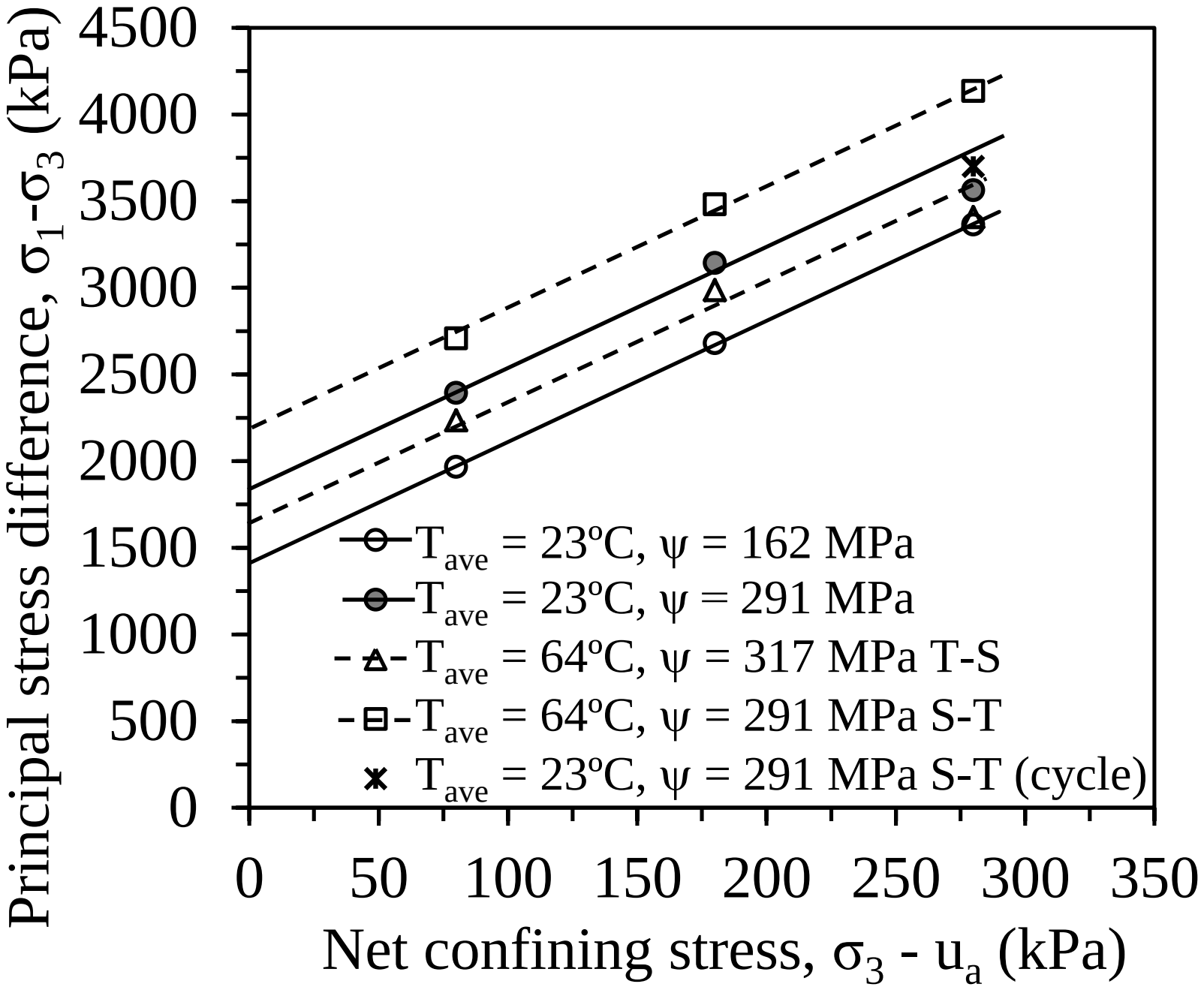
Principal stress difference, σ_1-σ_3 (kPa)
4500
4000
3500
3000
2500
2000
1500
1000
500
0
0
50
100
150
200
250
300
350
Net confining stress, σ_3 - u_a (kPa)
T_{ave} = 23ºC, ψ = 162 MPa
T_{ave} = 23ºC, ψ = 291 MPa
T_{ave} = 64ºC, ψ = 317 MPa T-S
T_{ave} = 64ºC, ψ = 291 MPa S-T
T_{ave} = 23ºC, ψ = 291 MPa S-T (cycle)

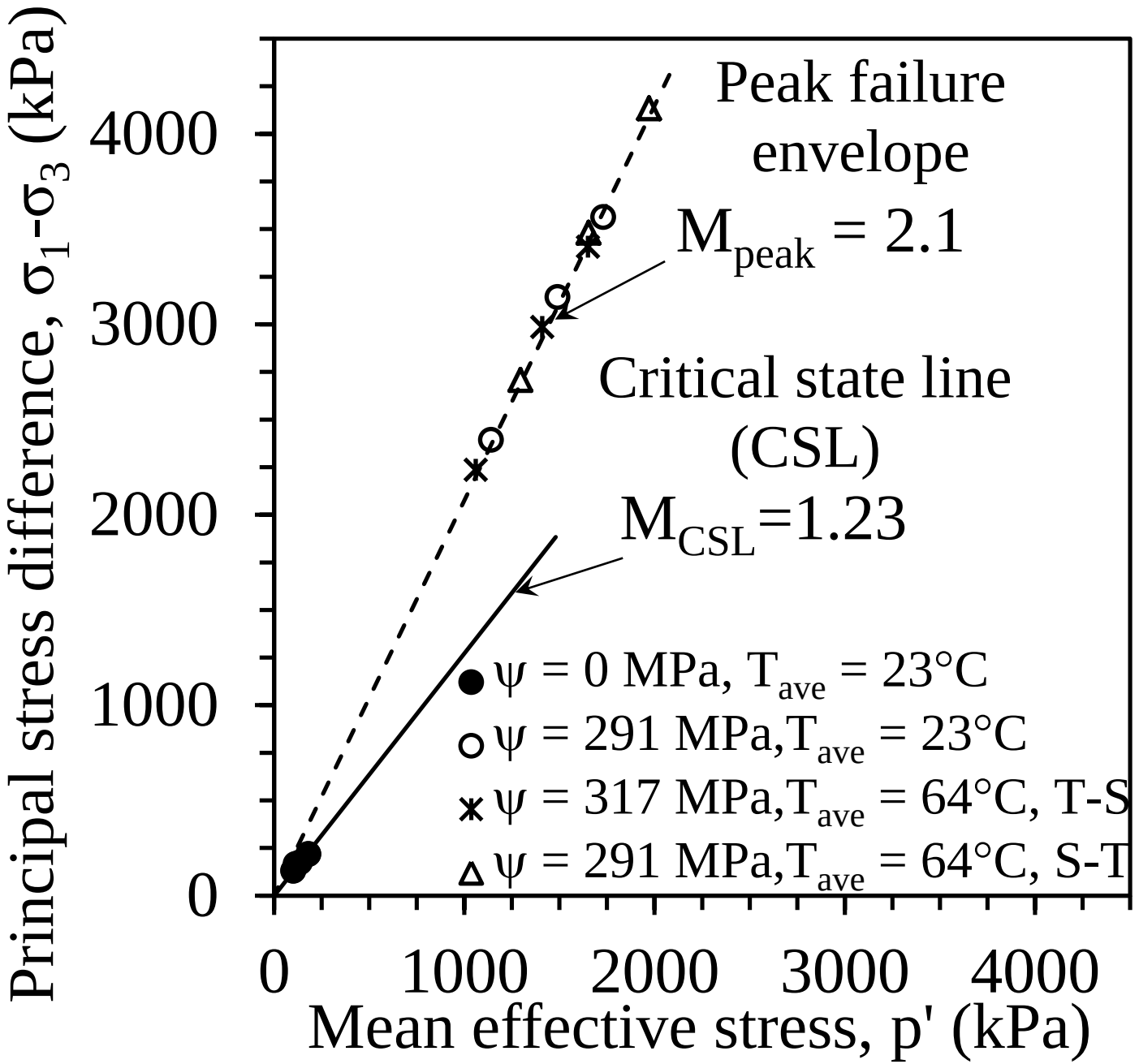
Principal stress difference, σ1-σ3 (kPa)
4000
3000
2000
1000
0
0
1000
2000
3000
4000
Mean effective stress, p' (kPa)
Peak failure envelope
Mpeak = 2.1
Critical state line (CSL)
MCSL=1.23
ψ = 0 MPa, Tave = 23°C
ψ = 291 MPa,Tave = 23°C
ψ = 317 MPa,Tave = 64°C, T-S
ψ = 291 MPa,Tave = 64°C, S-T

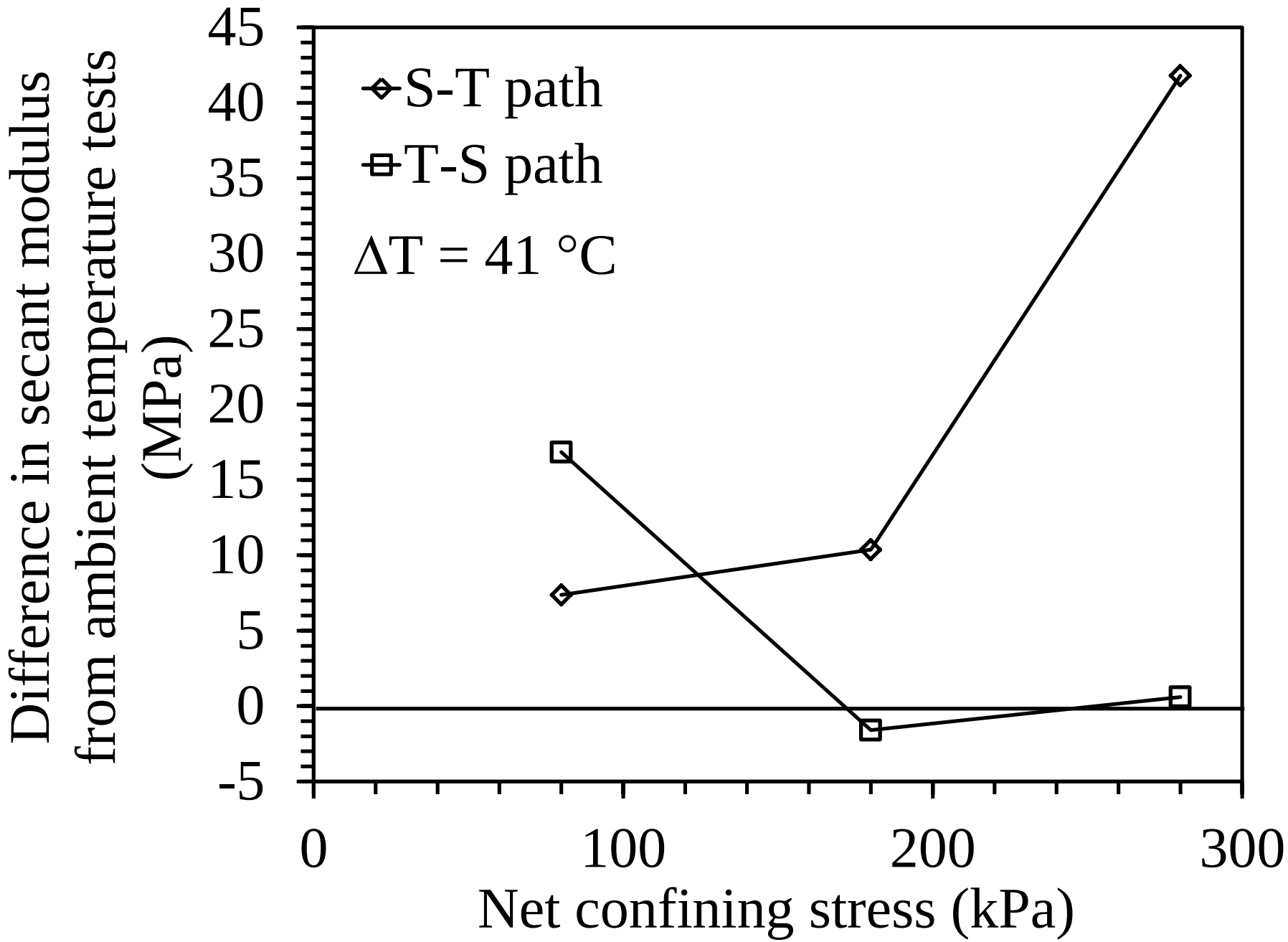
Difference in secant modulus from ambient temperature tests (MPa)
45
40
35
30
25
20
15
10
5
0
-5
S-T path
T-S path
ΔT = 41 °C
0
100
200
300
Net confining stress (kPa)

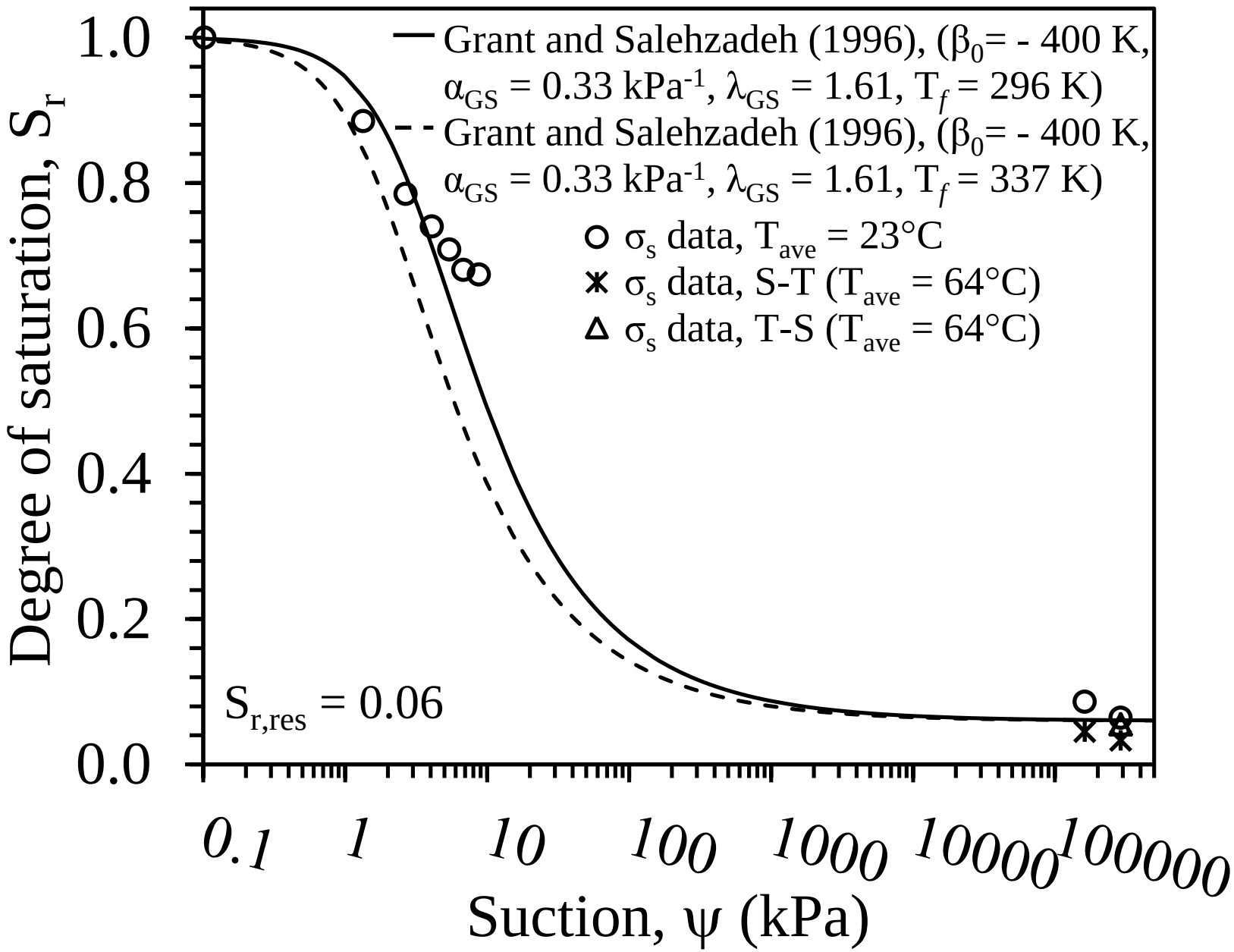
Grant and Salehzadeh (1996), (β_0= - 400 K, α_{GS} = 0.33 kPa^{-1}, λ_{GS} = 1.61, T_f = 296 K)
Grant and Salehzadeh (1996), (β_0= - 400 K, α_{GS} = 0.33 kPa^{-1}, λ_{GS} = 1.61, T_f = 337 K)
σ_s data, T_{ave} = 23°C
σ_s data, S-T (T_{ave} = 64°C)
σ_s data, T-S (T_{ave} = 64°C)
$S_{r,res}$ = 0.06
Degree of saturation, S_r
1.0
0.8
0.6
0.4
0.2
0.0
0.1
1
10
100
1000
10000
100000
Suction, ψ (kPa)

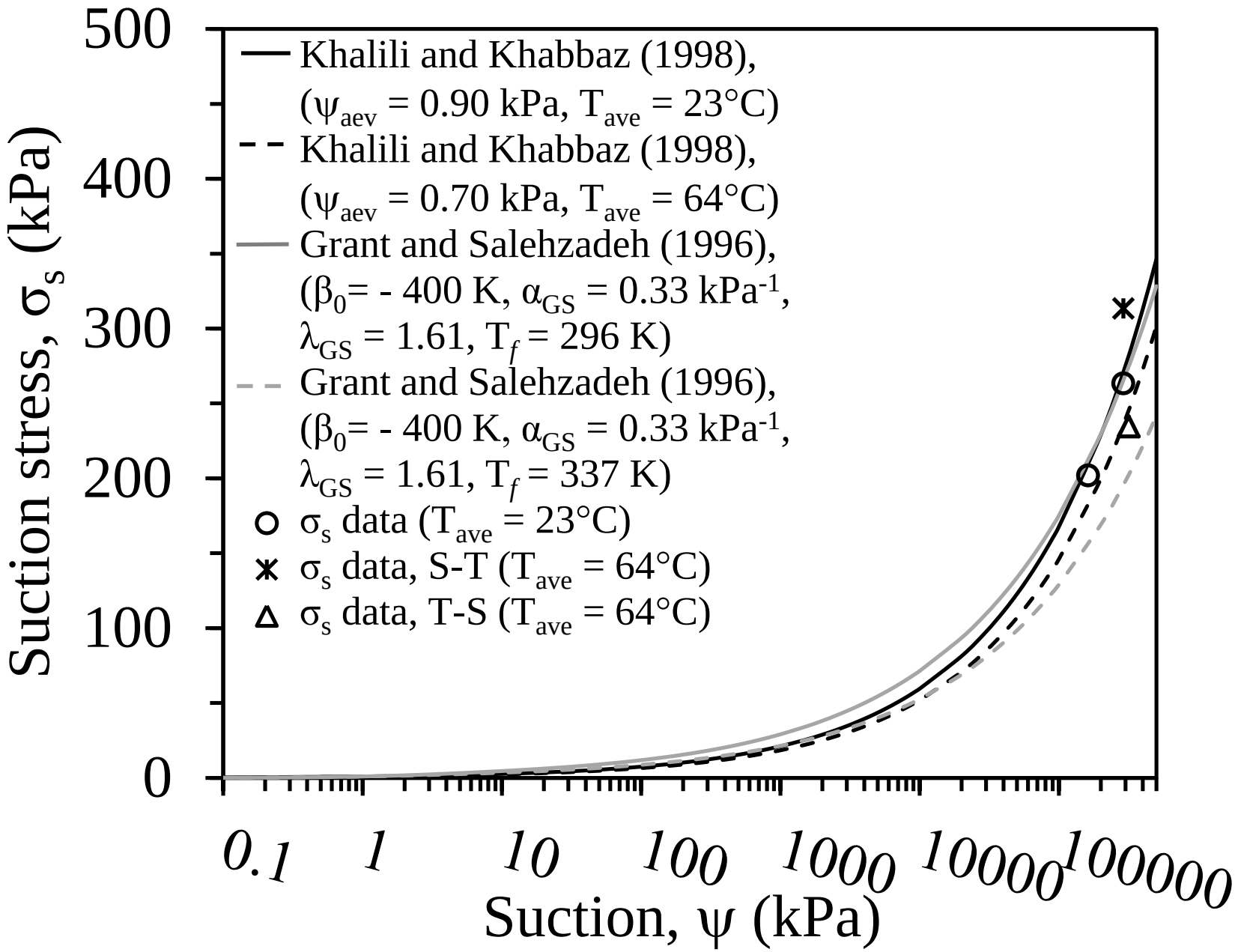
Suction stress, σ_s (kPa)
500
400
300
200
100
0
Khalili and Khabbaz (1998),
(ψ_{aev} = 0.90 kPa, T_{ave} = 23°C)
Khalili and Khabbaz (1998),
(ψ_{aev} = 0.70 kPa, T_{ave} = 64°C)
Grant and Salehzadeh (1996),
(β_0= - 400 K, α_{GS} = 0.33 kPa^{-1},
λ_{GS} = 1.61, T_f = 296 K)
Grant and Salehzadeh (1996),
(β_0= - 400 K, α_{GS} = 0.33 kPa^{-1},
λ_{GS} = 1.61, T_f = 337 K)
σ_s data (T_{ave} = 23°C)
σ_s data, S-T (T_{ave} = 64°C)
σ_s data, T-S (T_{ave} = 64°C)
0.1
1
10
100
1000
10000
100000
Suction, ψ (kPa)

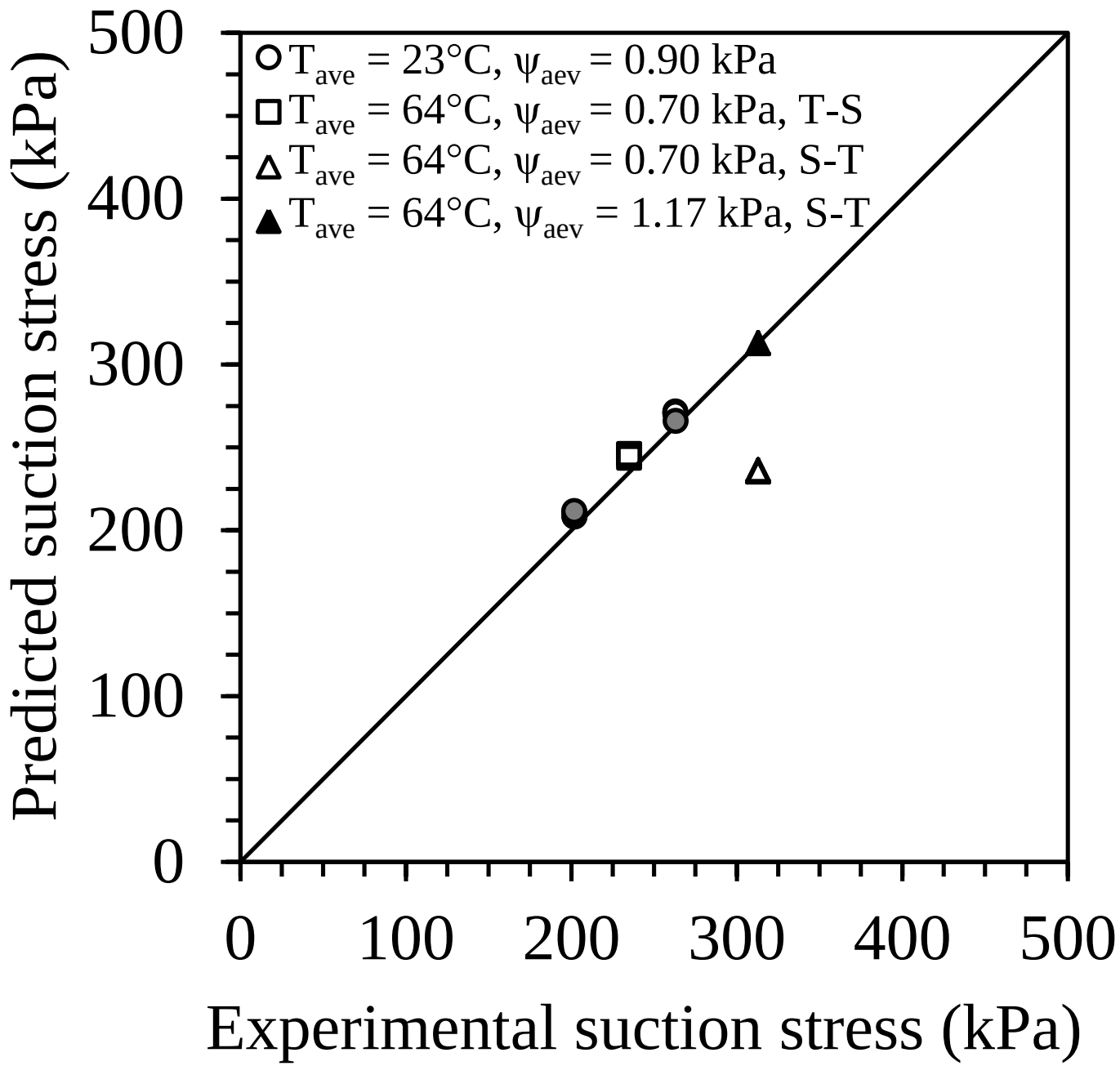
Predicted suction stress (kPa)
Experimental suction stress (kPa)
0
100
200
300
400
500
T_{ave} = 23°C, ψ_{aev} = 0.90 kPa
T_{ave} = 64°C, ψ_{aev} = 0.70 kPa, T-S
T_{ave} = 64°C, ψ_{aev} = 0.70 kPa, S-T
T_{ave} = 64°C, ψ_{aev} = 1.17 kPa, S-T